



# Unraveling the complexities of land transformation and its impact on urban sustainability through land surface temperature analysis

Saleha Jamal<sup>1</sup> · Mohd Saqib<sup>1</sup> · Wani Suhail Ahmad<sup>1,2</sup> · Manal Ahmad<sup>1</sup> · Md Ashif Ali<sup>1</sup> · Md Babor Ali<sup>1</sup>

Received: 8 May 2023 / Accepted: 6 August 2023 / Published online: 29 August 2023  
© The Author(s), under exclusive licence to Società Italiana di Fotogrammetria e Topografia (SIFET) 2023

## Abstract

Due to the ongoing population increase over the past years, fast and unchecked urbanization has been occurring in the urban centers of developing nations like India. As a result, land transformation is taking place at a fast pace leading to the creation of urban heat island (UHI). Urban heat island (UHI) constitutes a significant human alteration to the Earth system. Hence, this study presents a rigorous and comprehensive analysis of the impact of land use and cover on land surface temperature (LST) in Aligarh City, Uttar Pradesh, India, using multi-dimensional satellite data. The research collected Landsat data for four different phases (1991, 2001, 2011, and 2021) and analyzed it in conjunction with land use and cover (LULC) data to identify trends and variations. The result shows a consistent increase in LST since 1991, with built-up and bare land areas exhibiting the highest temperatures across all phases. Moreover, the study found that impervious land had the most significant effect on LST, followed by water bodies and vegetation cover. The analysis of the proportion of the area with the lowest and highest LST showed interesting trends, with a greater portion of Aligarh City experiencing a temperature range between 15 and 16 °C in 2021 compared to previous years. However, the study also found that 13.55% of the area had a maximum LST of over 17 °C, which is higher than the previous measurement of 9.04%, and has been steadily increasing since 1991. The accuracy of the study was verified by detecting elevated temperatures in non-porous areas and cooler temperatures near green zones and water bodies. This study's contribution to the research community lies in the data-driven, systematic analysis of the complex relationship between land use and cover and LST in an urban environment. The study's findings suggest that alterations in land use/cover patterns have a significant impact on LST, which has important implications for urban planning policies. The research provides valuable insights for urban planners, policymakers, and city officials, as it highlights the need for sustainable and efficient urban planning policies to mitigate the effects of urban heat islands and rising temperatures. The study's results have broader implications beyond Aligarh City and can inform land-use planning and policymaking in other cities facing similar challenges. This research presents a comprehensive analysis that can serve as a framework to inform land-use planning and policymaking, contributing to the development of sustainable and efficient urban environments.

**Keywords** Urbanization impacts · LST · NDBI · LULC · Spatial analysis · Urban planning and sustainability

---

✉ Wani Suhail Ahmad  
wanisuhailgeo@gmail.com

Saleha Jamal  
salehajm@gmail.com

Mohd Saqib  
saqibalg98@gmail.com

Manal Ahmad  
manalah1807@gmail.com

Md Ashif Ali  
asif4u.amu@gmail.com

Md Babor Ali  
baboraliamu@gmail.com

<sup>1</sup> Department of Geography, Aligarh Muslim University, Aligarh, India

<sup>2</sup> Department of Geography, University of Ladakh, Ladakh, India

## Introduction

Urbanization refers to the movement of people from rural areas to urban, suburban, or urbanized settings (Thomas et al. 2013). This shift has led to an increase in the number of metropolitan regions and population density in cities. In recent decades, the rate of urbanization has accelerated, and currently, over 56% of the world's population resides in urban areas, with that percentage projected to reach 68% by 2050 (UN-Habitat 2020). India, China, and Nigeria are expected to account for most of the projected 35% increase in the urban population from 2018 to 2050, with India expected to add 416 million additional urban dwellers, China adding 255 million, and Nigeria adding 189 million (United Nations, 2018).

However, rapid urbanization is not without its negative impacts. Research has shown that Indian cities, for example, are experiencing harmful effects from urbanization, including environmental and health concerns (Singh et al. 2017; Ahmad et al. 2022). As a result, monitoring and measuring land use and land cover (LULC) in urban areas have become critical in addressing the effects of urbanization. LULC alterations are considered the most significant human-induced environmental disturbance at the local level, leading to microclimate changes (Meyer and Turner, 1992; Roberts et al. 1998). Remote sensing technology has enabled the provision of spatio-temporal data for tracking, mapping, and evaluating LULC changes, which is crucial for monitoring several elements of local and global climatic changes, hydrology, biodiversity preservation, and air pollution (Sahana et al. 2020; Khurshed et al. 2022).

With the combination of geographic information systems (GIS) and remote sensing data, researchers and investigators have a platform to quickly and affordably assess the impact of LULC transformations and transitions on the environment. Remote sensing technologies have the advantage of quick data capture for LULC data collection, and the information obtained can be effectively utilized to extract, examine, and anticipate future patterns by relying on past and present LULC changes (Mishra & Rai 2016; Jamal et al. 2022a; Behera et al. 2023). In summary, as urbanization continues to grow, monitoring and evaluating LULC changes using remote sensing technologies will play a crucial role in mitigating the harmful effects of urbanization on the environment and human health.

The transformation of vegetated surfaces into impervious ones and the conversion of vegetated and wetland areas into agricultural land or barren wastelands are leading to an increase in surface temperatures, which is the most pressing issue affecting the planet as a whole and

urban region in particular (Mallick et al. 2008; Pal and Akoma 2009). These alterations can significantly transform the atmosphere near urban areas, affecting various elements such as the absorption of solar energy, surface reflectivity, temperature of the surface, rate of evaporation, heat transfer to the soil, heat storage, and wind turbulence (Mallick et al. 2008). Therefore, they play a critical role in modifying environmental processes (Oke and Cleugh 1987; Weng et al. 2004).

For over 60 years, urban temperature rise and the development of urban heat islands (UHIs) have been a cause for concern, particularly in emerging nations like India, where rapid urbanization and a growing population have made the situation worse (Hulley et al. 2019; Naikoo et al. 2020). The land surface temperature (LST) of an area is mainly affected by changes in the land's surface, as buildings, roads, pavements, and other infrastructures absorb a substantial amount of incoming solar radiation. The heat generated by vehicles, factories, air conditioners, and other sources further contributes to the temperature of the surroundings (Shahfahad et al. 2021; Jamali et al. 2022). Extreme LST can alter local wind patterns and precipitation rates, affecting the local weather and climate and leading to various respiratory ailments caused by poor air quality resulting from cooling agents (H. Liu and Weng 2012; L. Liu and Zhang 2011). Therefore, it is essential to have a thorough understanding of the consequences of extreme LST in a city to help mitigate climate change and human adaptation efforts (Arnfield 2003; Imhoff et al. 2010; Zhao et al. 2014).

Due to increased urbanization in India over the past 50 years, many small towns have transformed into metropolises with populations larger than one million, leading to a large number of Indian cities experiencing the urban heat island (UHI) effect and land surface temperature (LST) effect (Tran et al. 2017; Shahfahad et al. 2021). Although housing and economic development are necessary to accommodate the growing population, the focus must be on reducing the consequences of LST and UHI and working towards sustainability. Therefore, understanding how changes in land cover affect LST and UHI over time is crucial (Shen et al. 2020; Talukdar et al. 2020). Today's cities are better defined as spreading areas connecting to one another in a dendritic pattern, with commercial development occurring along main thoroughfares and residential construction often on former agricultural lands. The urban heat island is being replaced by a broad and deep land transformation of the countryside, and this has been discussed in studies by Al-Sharif and Pradhan (2014), Arsanjani et al. (2013), and Sang et al. (2011) among others (Arora et al. 2004; Li and Yeh 2002).

This study focuses on investigating the impact of urbanization on Aligarh’s land surface temperature by analyzing changes in land use and land cover (LULC) in the specified area. The research question posed was whether there is a relationship between the transformation of land in Aligarh and the LST in the study area. The primary objective of the study was to analyze and assess changes in LULC in Aligarh City from 1991 to 2021 and to measure LST both qualitatively and statistically during this period. The results indicated significant changes in some LULC categories, and there was a frequent increase in the area’s surface temperature. Therefore, it is crucial to develop strategies to mitigate the effects of urbanization and reduce the LST effect to ensure the long-term sustainability of cities like Aligarh.

### Study area

Aligarh, a city located in the western region of Uttar Pradesh, northern India, boasts a rich history that dates back to various periods, including the Mughal, Maratha, and British rule (Sharma and Vashishtha 2023). The city spans across a total area of 98.5 km<sup>2</sup>, comprising of 90 wards, and is situated in a productive area between the Ganga and Yamuna rivers. Its UTM Zone is 44 N, and it experiences a tropical monsoon climate with uneven and inadequate precipitation, with annual rainfall ranging from 65 to 75 cm. The summers in Aligarh are characterized by extremely high temperatures, which can soar up to 46° C in June. The region’s topography is similar to other parts of the Gangetic plain, with a gentle slope from north to south and a swing to

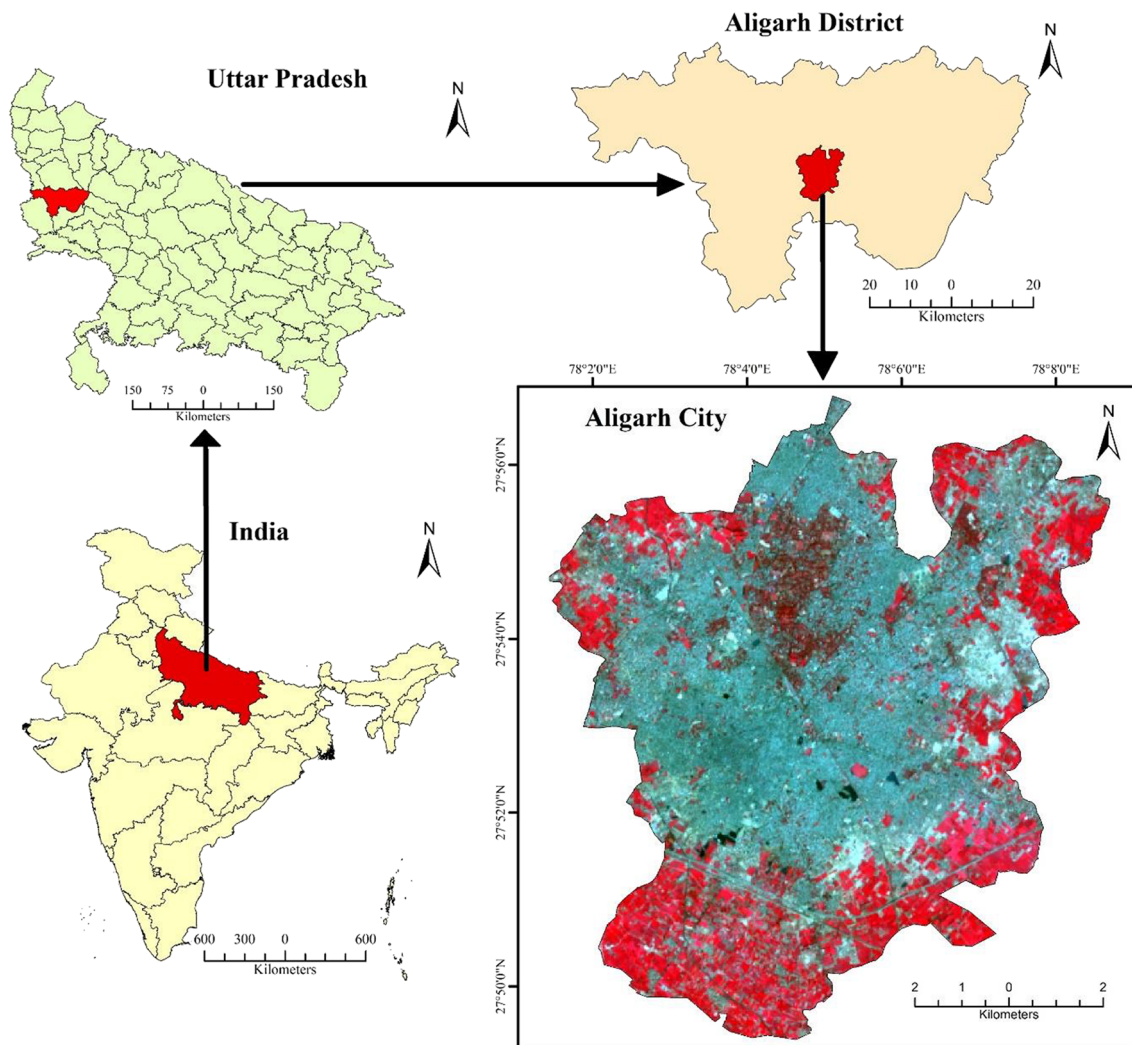


Fig. 1 Study area (Aligarh City)

**Table 1** The geo-spatial data used for the present study

Satellite	Sensor	Date	Resolution (m)	Path	Row	UTM Zone
Landsat 5	TM (Thematic mapper)	25-01-1991	30	146	041	43
Landsat 7	ETM+ (Enhanced thematic mapper plus)	28-01-2001	30	146	041	43
Landsat 5	TM (Thematic mapper)	16-01-2011	30	146	041	43
Landsat 8	OLI (Operational land imager)	27-01-2021	30	146	041	43

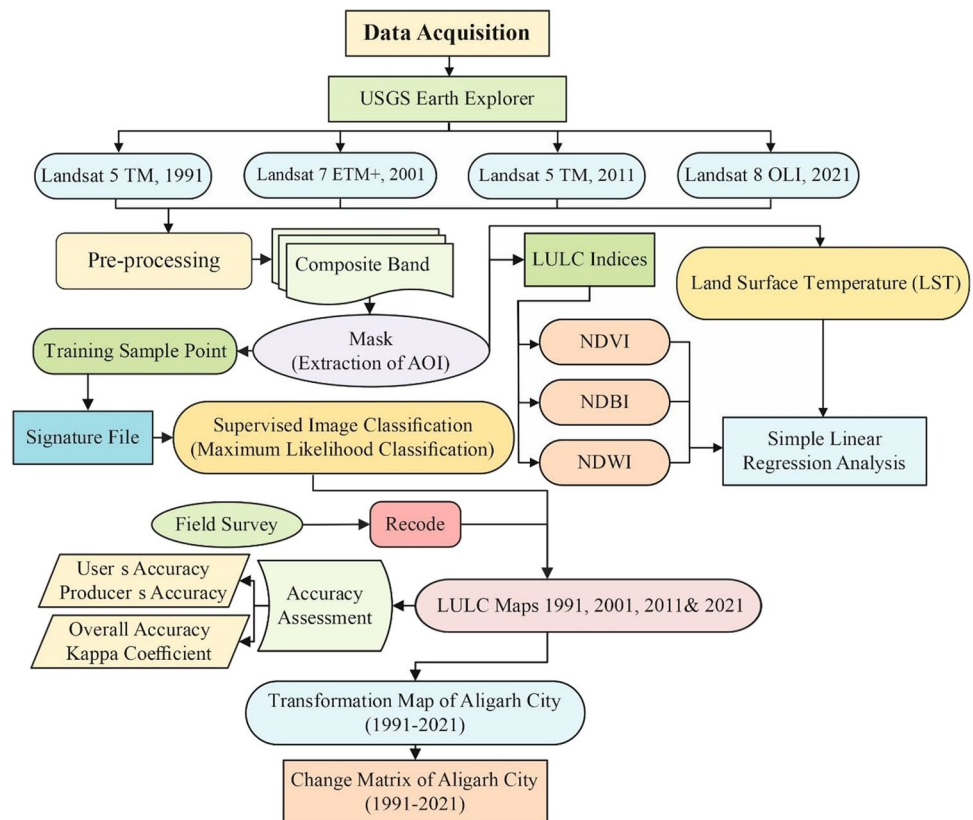
the southeast. The fertile alluvial soil in the region is primarily used for agriculture. The Aligarh district's fertile soil supports a thriving agricultural industry, while the lock industry serves as a significant source of employment for the city's population. However, population growth and urbanization have driven the continuous expansion of Aligarh City for decades (Fig. 1). A significant portion of previously vacant or agricultural land has been transformed into built-up areas, leading to an increase in the number of wards. As a result, the city's land use has undergone a significant change over the years. Furthermore, the land surface temperature in Aligarh has been steadily rising due to the growing population and the emergence of impervious surfaces, making the city vulnerable to the urban heat island effect.

## Database and methodology

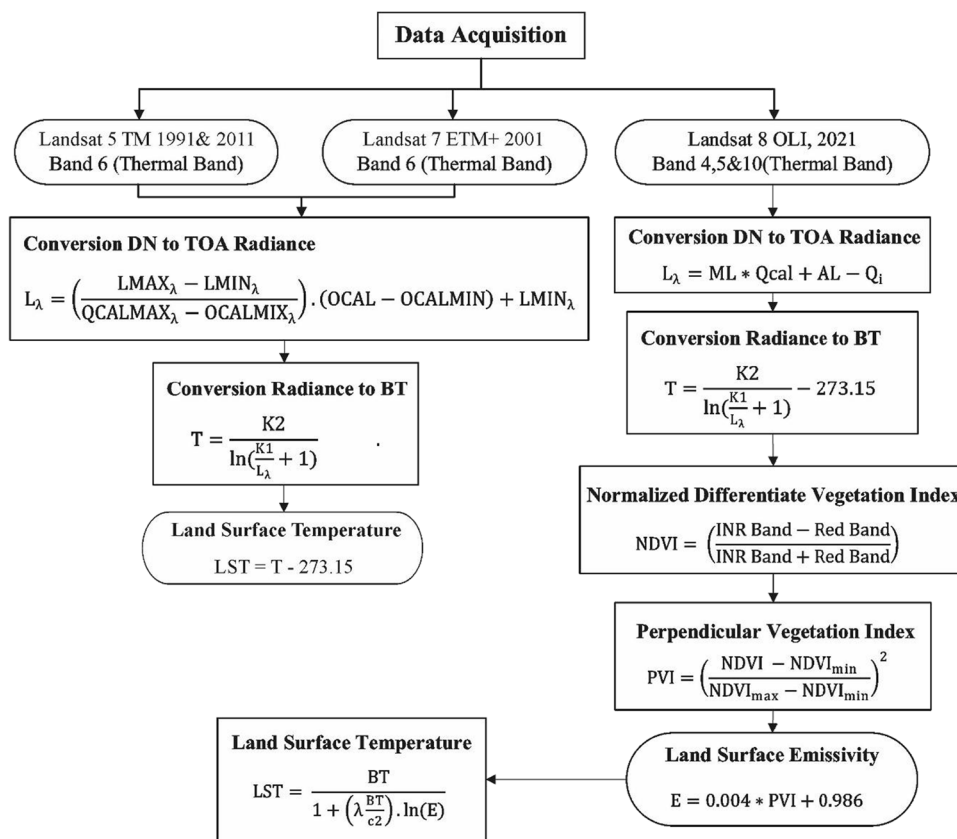
This research has been conducted through field surveys and geospatial satellite data. The satellite data were obtained from the USGS (United States Geological Survey) Earth Explorer, and the digital elevation model (DEM) was obtained from Bhuvan (ISRO's Indian Geo-platform). A field survey was also carried out for verification.

### Satellite data

According to Smith et al. (1998), remote sensing data and geographical information system techniques are very useful and accurate for monitoring wetland patterns due

**Fig. 2** Methodological flow-chart for LULC and LST

**Fig. 3** Methodological flowchart for retrieval of land surface temperature (LST)



to their synoptic and repetitive features. In this study, Landsat-5 TM, Landsat 7 ETM + , Landsat-5 TM, and Landsat-8 OLI data were used for the years 1991, 2001, 2011, and 2021, respectively. The satellites followed a path and row of 146 and 41, respectively, and all yearly images had a spatial resolution of 30 m. The satellite data was obtained from the United States Geological Survey Earth Explorer Web Portal. Turbulence-free atmospheric satellite images were chosen and then geo-referenced and rectified during the pre-processing stage, using the nearest neighbor resampling method for image registration. To achieve maximum overlay accuracy, 25 ground control points were taken, and the images were projected based on the WGS 84 datum and UTM Zone 43 N projection. More information on each image is provided in Table 1.

**Other data**

The current research utilized non-spatial information from the Census of India, as well as Google Maps and administrative and topographical maps of the study area to conduct the study. Table 1 shows the geo-spatial data used for the present study.

**Methods**

**(a) Pre-processing of imageries**

In order to enhance the accuracy of the results, the satellite images underwent geometric and radiometric corrections before undergoing further analysis. Once these corrections were applied, the images were coregistered and resampled to a uniform 30-m pixel resolution. Based on the band combination, a specific area of interest was selected to generate maps of land use/land cover, LULC indices, and land surface temperature (Fig. 2).

**Supervised classification method**

To create maps of land use/land cover, training samples were collected for each category according to the areal coverage of the particular class. These samples were compared with Google Earth and a topographical map to ensure accuracy in identifying built-up areas, crop land, fallow/bare land, plantation, vegetation, and water bodies. The supervised classification technique was then used to classify all images, utilizing the Maximum

**Fig. 4** Land use/land cover map of Aligarh City, 1991, 2001, 2011, and 2021

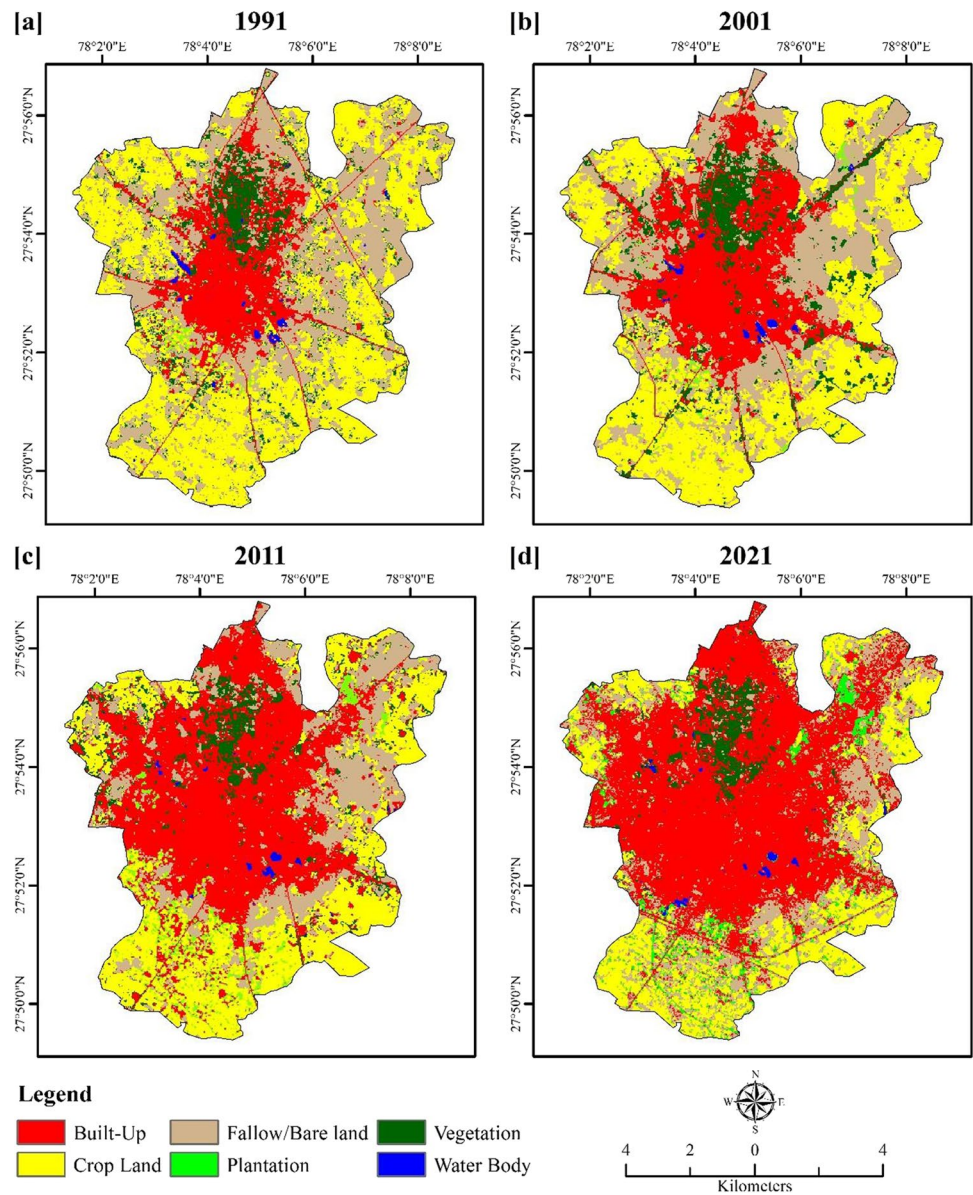


**Table 2** Area under different LULC and net change

Class name	1991		2001		2011		2021		Net change (1991–2021)	Growth (%)
	Area in Ha	Area (%)	Area in Ha	Area (%)	Area in Ha	Area (%)	Area in Ha	Area (%)		
Built-up	1539.99	15.62	2331.99	23.65	4097.61	41.55	5229.21	53.03	3689.22	239.56
Crop land	4019.01	40.76	3330.90	33.78	2683.62	27.21	1959.95	19.88	-2059.06	-51.23
Fallow/bare land	3373.37	34.21	3150.27	31.95	2021.31	20.50	1817.09	18.43	-1556.28	-46.13
Plantation	49.76	0.50	189.73	1.92	392.41	3.98	436.19	4.42	386.42	776.54
Vegetation	826.10	8.38	809.86	8.21	621.72	6.30	378.13	3.83	-447.97	-54.23
Water body	52.97	0.54	48.46	0.49	44.54	0.45	40.64	0.41	-12.33	-23.28
Total	9861.21	100	9861.21	100	9861.21	100	9861.21	100		

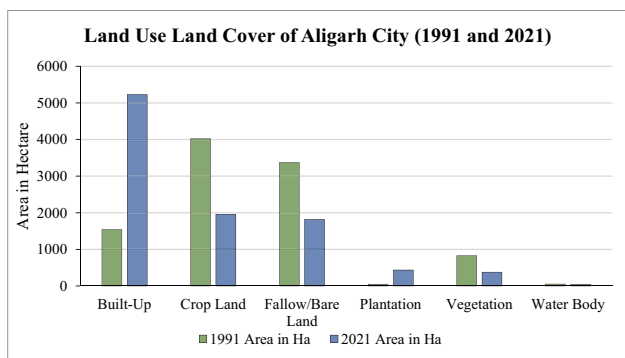


**Fig. 5** Area under different LULC classes (1991, 2001, 2011, and 2021)

Likelihood Classifier Algorithm. Two sets of imagery from different time intervals were classified using this technique and algorithm. The software programs ERDAS IMAGINE 2015 and ArcMap 10.5 were utilized for image processing and map preparation in this study (Jamal and Ahmad 2020; Vinayak et al. 2022).

### LULC change detection method

To analyze changes in land use/land cover over a period of three decades, the values for each individual category were used to calculate the rate of change using the equation below, as described by Puyravaud (2003), Rahaman et al. (2019), and Ganaie et al. (2021).

$$R = [1/(t1 - t2)] \times [\ln(C1/C2)] \tag{1}$$

In this equation, *R* represents the rate of change in LULC, while *C1* and *C2* represent the areas covered by LULC categories during time periods *t1* (the most recent year) and *t2* (the previous year), respectively.

### Retrieving of land surface temperature from Landsat data

Land surface temperature (LST) refers to the temperature of the surface of the Earth’s land (Abbas et al. 2021). It differs from air temperature and can be affected by factors such as vegetation, soil type, and urbanization. LST

**Fig. 6** Growth in different LULC classes (1991, 2001, 2011, and 2021)

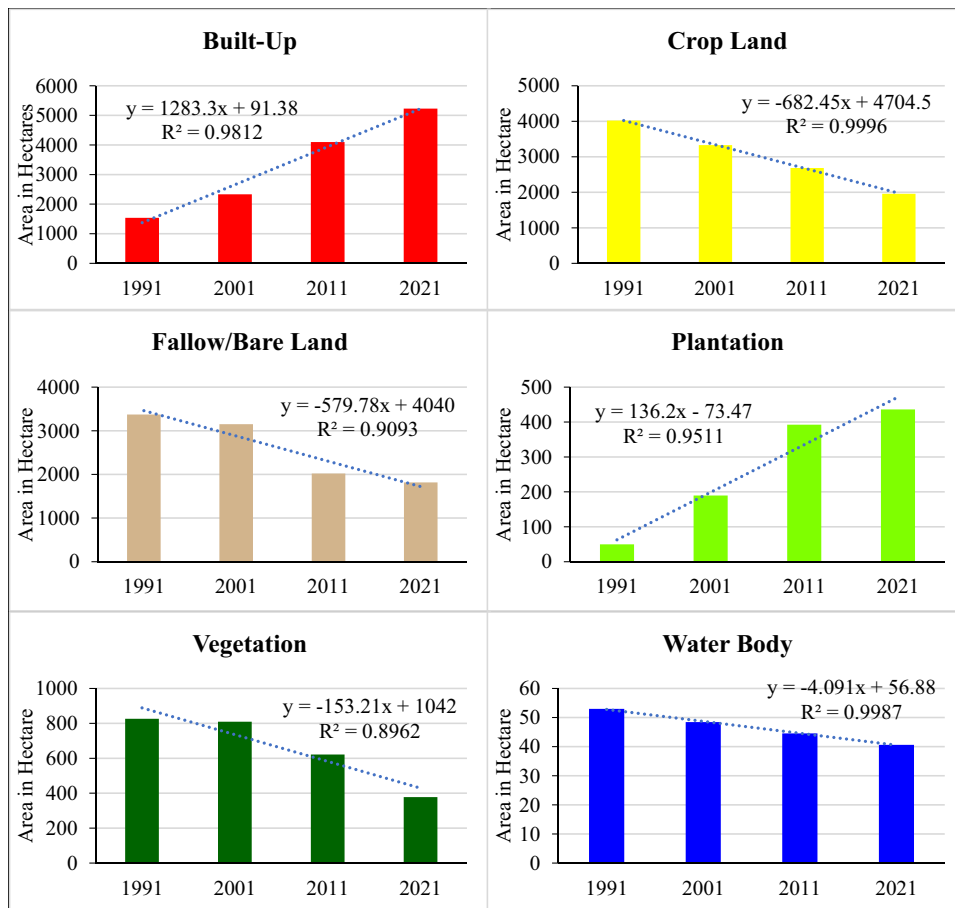


**Table 3** Transformation matrix of LULC of Aligarh City (1991–2021)

Class Name	2021							
	B	C	F	P	V	W	RT	
1991	B	1539.99	0.00	0.00	0.00	0.00	0.00	1539.99
	C	1147.08	1559.41	993.15	259.46	52.27	7.63	4019.01
	F	2084.34	310.80	709.03	139.76	111.34	18.10	3373.37
	P	42.08	0.66	3.05	2.36	0.55	1.05	49.76
	V	383.23	88.10	106.97	33.15	212.58	2.07	826.10
	W	32.49	0.98	4.88	1.46	1.38	11.79	52.97
	CT	5229.21	1959.95	1817.09	436.19	378.13	40.64	9861.21

CT column total, W water body, RT row total, C crop land, PA producer’s accuracy, B built-up, UA user’s accuracy, F fallow land

can be measured using remote sensing techniques, such as thermal infrared imaging. It is an important variable in understanding and predicting weather patterns, studying land–atmosphere interactions, and exploring the effects of land use changes on the climate.

In this study, the mono-window technique described by Qin et al. (2001) was used to obtain land surface temperature (LST) data from multiple Landsat satellite sensors over time. This method requires specific parameters, including ground emissivity, atmospheric transmittance, and effective mean atmospheric temperature. Initially, the original thermal infrared (TIR) bands, with resolutions of 100 m for Landsat 8 OLI data and 120 m for Landsat 5 TM data were resampled to a 30-m resolution by the USGS data center for subsequent analysis.

### Calculation of LST from thermal band of Landsat 5 TM and Landsat 7 ETM +

#### Conversion digital number (DN) to top of atmosphere (TOA) spectral radiance

To convert the spectral radiance of each thermal band into brightness temperature, Eq. (2) was used:

$$L_{\lambda} = ((L_{max\lambda} - L_{min\lambda}) / (Q_{cal\_max} - Q_{cal\_min})) \times (Q_{cal} - Q_{cal\_min}) + L_{min\lambda} \tag{2}$$

Here,  $L_{\lambda}$  represents spectral radiance, while  $Q_{cal}$  represents the quantized calibrated pixel value in DN.  $L_{max\lambda}$  refers to spectral radiance scaled to  $Q_{cal\_max}$  (in Watts/m<sup>2</sup> \* sr \* μm), and  $L_{min\lambda}$  refers to spectral radiance scaled to  $Q_{cal\_min}$ .

**Fig. 7** Transformation map of Aligarh City (1991–2021)

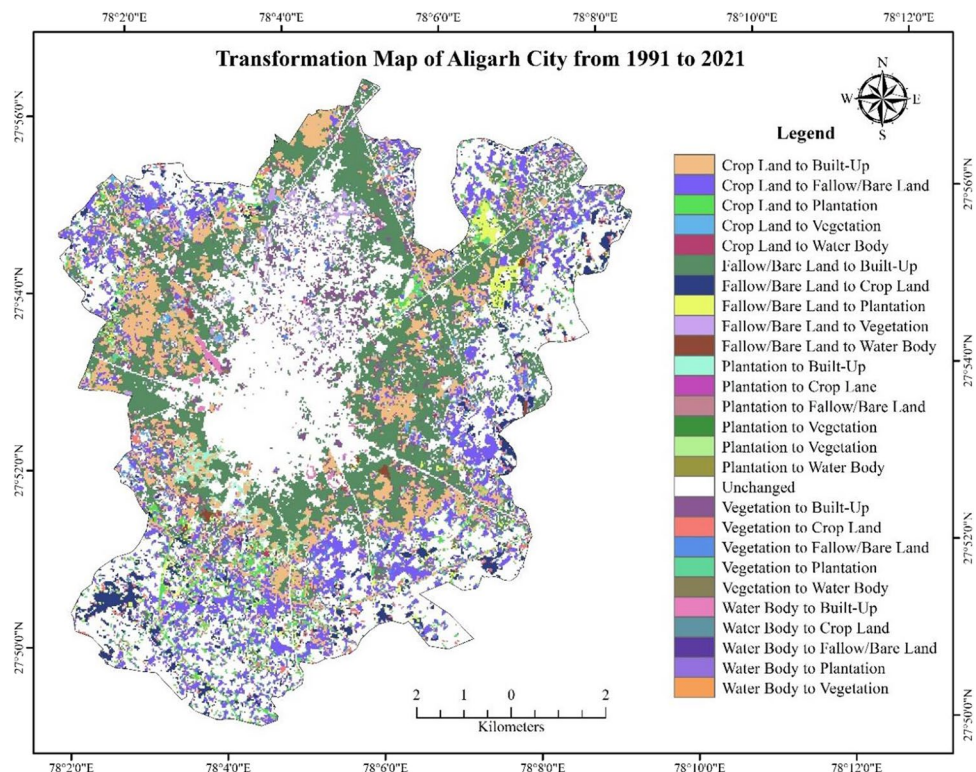




**Table 4** Error matrix and total accuracy of Aligarh City

Year	Class	W	C	B	F	V	P	RT	UA (%)
1991	W	9	1	0	0	1	0	11	81.82
	C	0	20	0	0	4	1	25	80.00
	B	0	0	13	5	0	0	18	72.22
	F	0	0	2	18	0	0	20	90.00
	V	0	2	0	0	11	2	15	73.33
	P	0	1	0	0	1	9	11	81.82
	CT	9	24	15	23	17	12	100	
PA (%)	100.00	83.33	86.67	78.26	64.71	75.00			
2001	W	9	0	0	0	1	0	10	90.00
	C	0	21	1	0	1	1	24	87.50
	B	0	0	16	3	0	0	19	84.21
	F	0	0	4	19	0	0	23	82.61
	V	0	2	0	0	9	1	14	78.57
	P	0	1	0	0	1	9	10	90.00
	CT	9	24	21	22	13	11	100	
PA (%)	100.00	87.50	76.19	86.36	84.62	81.82			
2011	W	9	0	0	0	1	0	10	90.00
	C	0	19	0	0	1	1	21	90.48
	B	0	0	24	3	0	0	27	88.89
	F	0	0	2	16	0	0	18	88.89
	V	0	1	0	0	9	2	12	75.00
	P	0	1	0	0	1	10	12	83.33
	CT	9	21	26	19	12	13	100	
PA (%)	100.00	90.48	92.31	84.21	75.00	76.92			
2021	W	9	0	0	0	1	0	10	90.00
	C	0	12	0	1	0	0	13	92.31
	B	0	1	35	1	2	0	39	89.74
	F	0	1	2	11	0	0	14	78.57
	V	0	1	0	0	12	1	14	85.71
	P	0	1	0	0	1	8	10	80.00
	CT	9	16	37	13	16	9	100	
PA (%)	100.00	75.00	94.59	84.62	75.00	88.89			

1991 = Number corrected 80; Classified total 100; Overall Accuracy 80%; Overall Kappa Statistics 0.7433  
 2001 = Number corrected 85; Classified total 100; Overall Accuracy 85%; Overall Kappa Statistics 0.8157  
 2001 = Number corrected 87; Classified total 100; Overall Accuracy 87%; Overall Kappa Statistics 0.8400  
 2021 = Number corrected 88; Classified total 100; Overall Accuracy 88%; Overall Kappa Statistics 0.8270

CT column total, W water body, RT row total, C crop land, PA producer’s accuracy, B built-up, UA user’s accuracy, F fallow/bare land, V vegetation, P plantation

**Convert radiance into brightness temperature/land surface temperature**

The conversion of top of atmosphere (TOA) radiance or spectral radiance to brightness temperature is a common process in remote sensing and satellite meteorology. This conversion is necessary because the data collected by satellite sensors is typically in the form of radiance, but for many applications, it is more useful to have this data in the form of temperature.

The conversion is based on the principle of Planck’s law, which describes the spectral radiance of

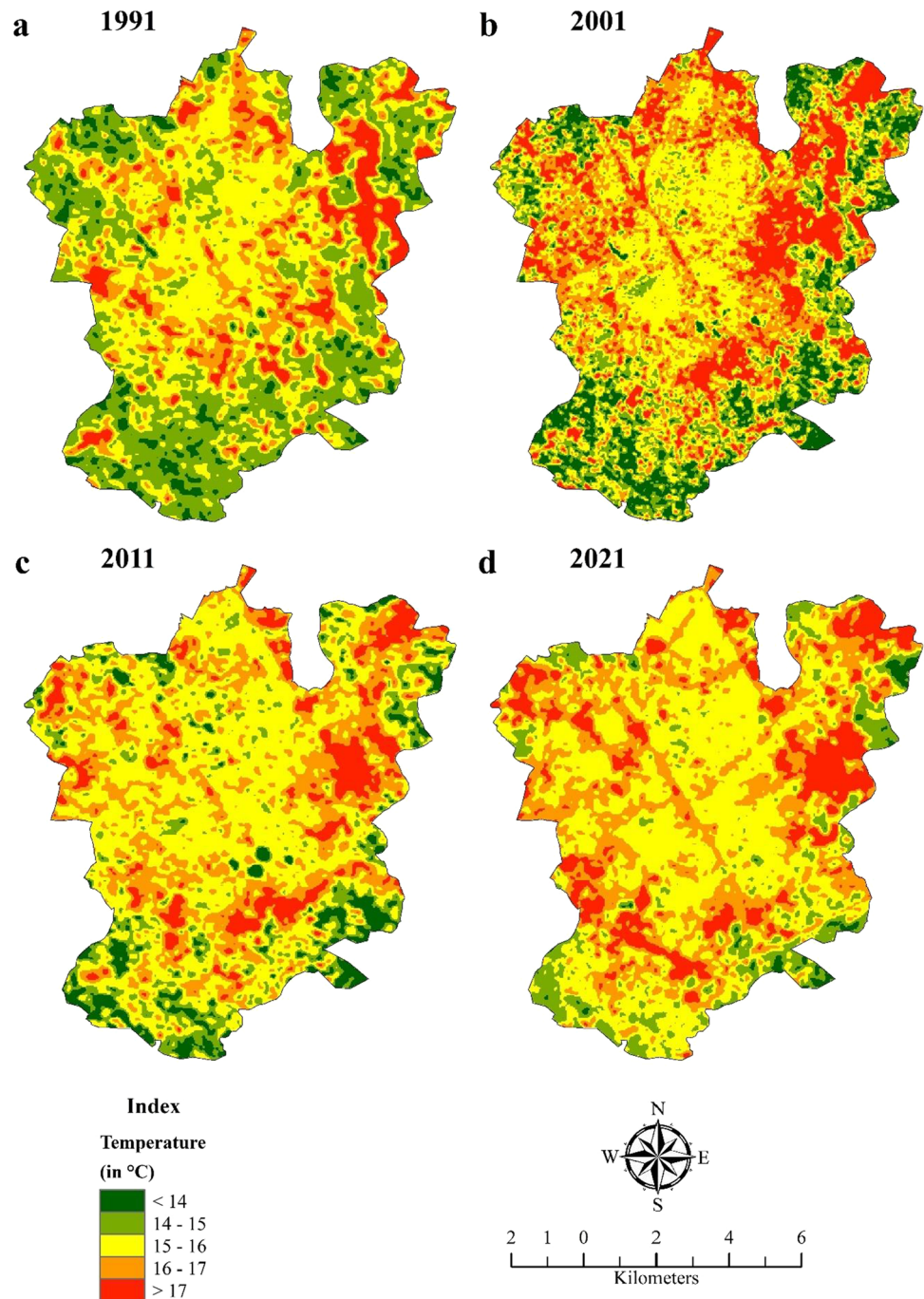
electromagnetic radiation at all wavelengths from a black body at temperature T.

**Calculation of LST from thermal band of Landsat 8 OLI**

**Conversion digital number (DN) to top of atmosphere (TOA) spectral radiance**

Initially, the thermal infrared digital numbers were converted to top of atmosphere (TOA) spectral radiance

**Fig. 8** Land surface temperature (LST) of Aligarh City (**a** 1991, **b** 2001, **c** 2011, and **d** 2021)



using the “radiance rescaling factor” proposed by Cohen (1960). Equation (4) was used:

$$L_{\lambda} = ML \times Q_{cal} + AL - Q_i \quad (3)$$

Here,  $L_{\lambda}$  represents TOA spectral radiance (in watts/ $m^2 \cdot sr \cdot \mu m$ ), ML represents the radiance multiplicative band, AL represents the radiance add band,  $Q_{cal}$  represents the quantized and calibrated standard product pixel

value (in DN), and  $Q_i$  represents the correction value for band 10, which is 0.29.

**Conversion of top of atmosphere (TOA)/spectral radiance to brightness temperature**

$$T = \frac{K_2}{\ln\left(\frac{K_1}{L_{\lambda}} + 1\right)} \quad (4)$$

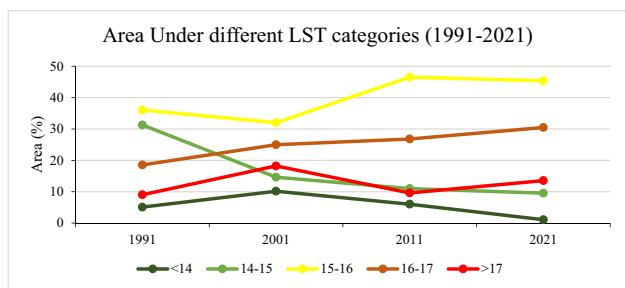


Fig. 9 Spatial trend showing the area under different LST categories

In this equation,  $T$  refers to the at-satellite brightness temperature,  $L_{\lambda}$  refers to the top of atmosphere spectral radiance, and  $K1$  and  $K2$  are constant values specific to the band being analyzed.

**Proportion of vegetation (PV)**

It is calculated using Eq. (6) (Jamal et al. 2022b):

$$PV = \left( \frac{NDVI - NDVI_{min}}{NDVI_{max} - NDVI_{min}} \right)^2 \tag{5}$$

**Land surface emissivity**

NDVI (Normalized Difference Vegetation Index) is a characteristic of natural objects and is a crucial surface parameter

derived from the radiance emitted by a specific location. The NDVI values are utilized to evaluate the average emissivity of an element present on the Earth’s surface. The mathematical representation of this is given by Eq. (7).

$$E = 0.004 \times PV + 0.986 \tag{6}$$

**Land surface temperature (LST)**

The output obtained after conducting all the aforementioned calculations is the average temperature derived from the observed radiance of an object present on the Earth’s surface. This is represented by Eq. (8).

$$LST = \left( \frac{BT}{1} \right) + W \left( \frac{BT}{14280} \right) * \ln(E) \tag{7}$$

The formula to compute the land surface temperature (LST) is given by Eq. (7), where LST is determined using the at-satellite brightness temperatures (BT) and the wavelength of emitted radiance ( $W$ ). The equation also involves the natural logarithm of emissivity ( $E$ ) and a constant value of 14,280 (Fig. 3).

**Conversion of LST data from Kelvin to degree Celsius**

Once all the five steps were completed, the LST data was obtained in Kelvin. Since this unit is not commonly used, the data was converted to the Celsius scale (°C) for ease of

Fig. 10 Cross profile of LST (AA', BB', and CC') drawn over LST of Jan. 1991 and Jan. 2021

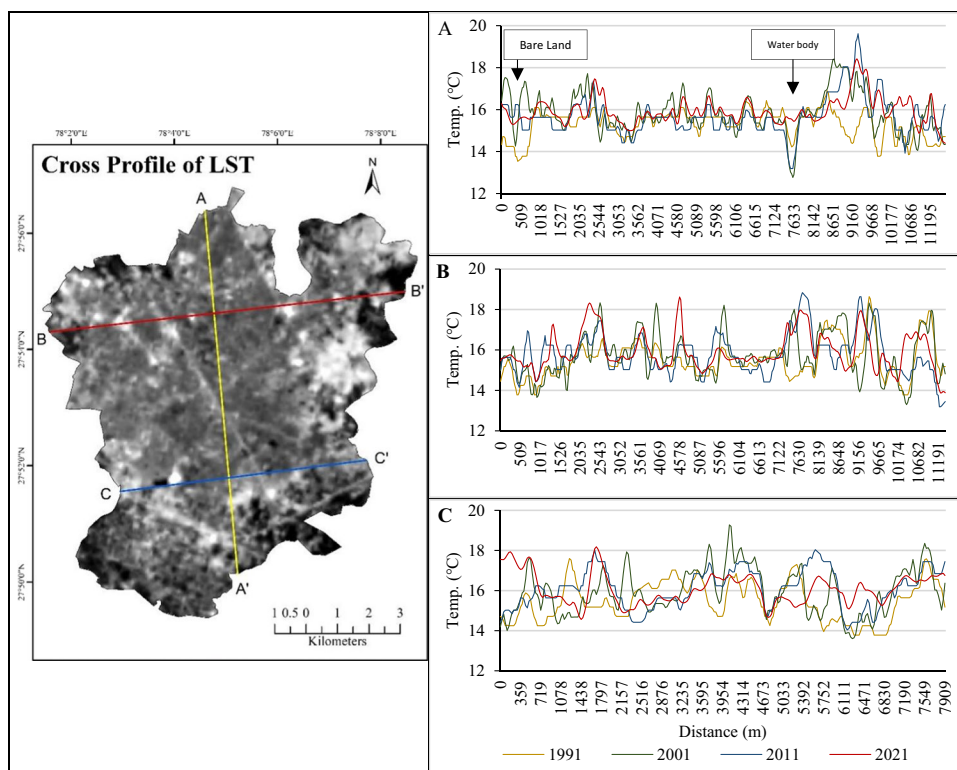
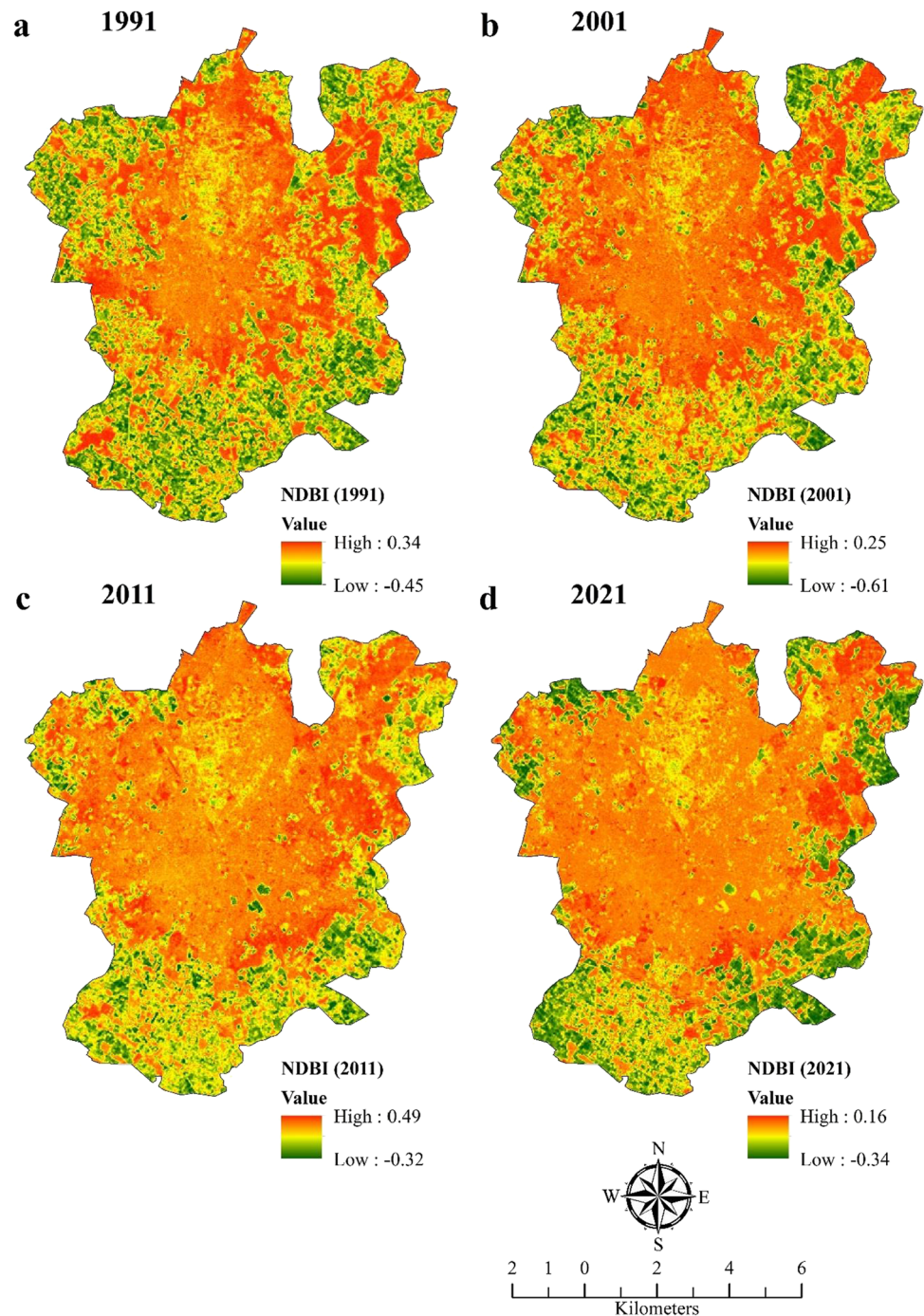


**Fig. 11** Normalized Differentiate Built-up Index (NDBI) of Aligarh City (1991, 2001, 2011, and 2021)



understanding. To convert from Kelvin to Celsius, the value at satellite brightness temperature was subtracted from 273.15 K.

### Calculation of LULC indices (NDVI, MNDWI, NDBI, and NDBal)

#### Normalized Difference Vegetation Index (NDVI)

NDVI is a metric that quantifies the density of vegetation in a region based on the reflectance of light by plants in the

near-infrared and red parts of the electromagnetic spectrum. It ranges between  $-1$  and  $1$ , with larger values indicating greater vegetation coverage. NDVI is a useful tool for monitoring crop growth and tracking variations in vegetation patterns over time. It is widely utilized in the fields of agriculture and remote sensing. It can be expressed in the following:

$$\text{NDVI} = \frac{\text{NIR (near infrared)band} - \text{red band}}{\text{NIR (near infrared) band} + \text{red band}} \quad (8)$$

**Fig. 12** Plot of NDBI vs LST with coefficient of determination ( $R^2$ ) for different time periods

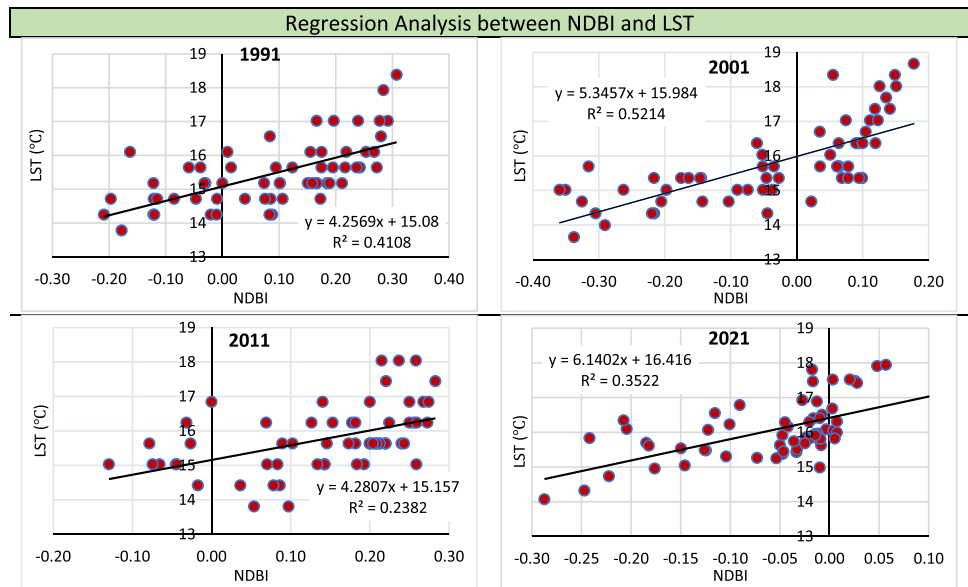


**Table 5** Coefficient of variation of temperature in selected time periods

Month	Year	Minimum	Maximum	Mean	Mean decadal change	Standard deviation	Coefficient of variation (%)
January	1991	12.84	20.18	15.38	-	1.00	6.50
January	2001	12.60	20.27	15.69	0.31	1.2	7.63
January	2011	12.57	20.41	15.73	0.04	1.05	6.69
January	2021	13.40	21.40	16.00	0.27	0.91	5.68

**Modified Normalized Difference Water Index (MNDWI)**

MNDWI is a tool utilized to assess water bodies. NDWI values can fluctuate between  $-1$  and  $+1$ ; since in the case of water bodies, the green band has a greater reflectance than the near-infrared.

$$MNDWI = \frac{Green - SWIR \text{ (short wave infrared)}}{Green + SWIR \text{ (short wave infrared)}} \quad (9)$$

**Normalized Difference Built-up Index (NDBI)**

NDBI is a measure used to classify and map built-up areas, such as urban areas, using remote sensing data. NDBI is calculated using the difference in reflectance between two spectral bands, typically the short-wave infrared (SWIR) and the near-infrared (NIR) bands.

$$NDBI = \frac{SWIR \text{ band} - NIR \text{ band}}{SWIR \text{ band} + NIR \text{ band}} \quad (10)$$

where: SWIR = short-wave infrared NIR = near infrared

**Normalized Difference Bareness Index (NDBaI)**

NDBaI employed to detect bare land in the study area.

$$NDBaI = \frac{SWIR - TIR \text{ (thermal infrared)}}{SWIR + TIR \text{ (thermal infrared)}} \quad (11)$$

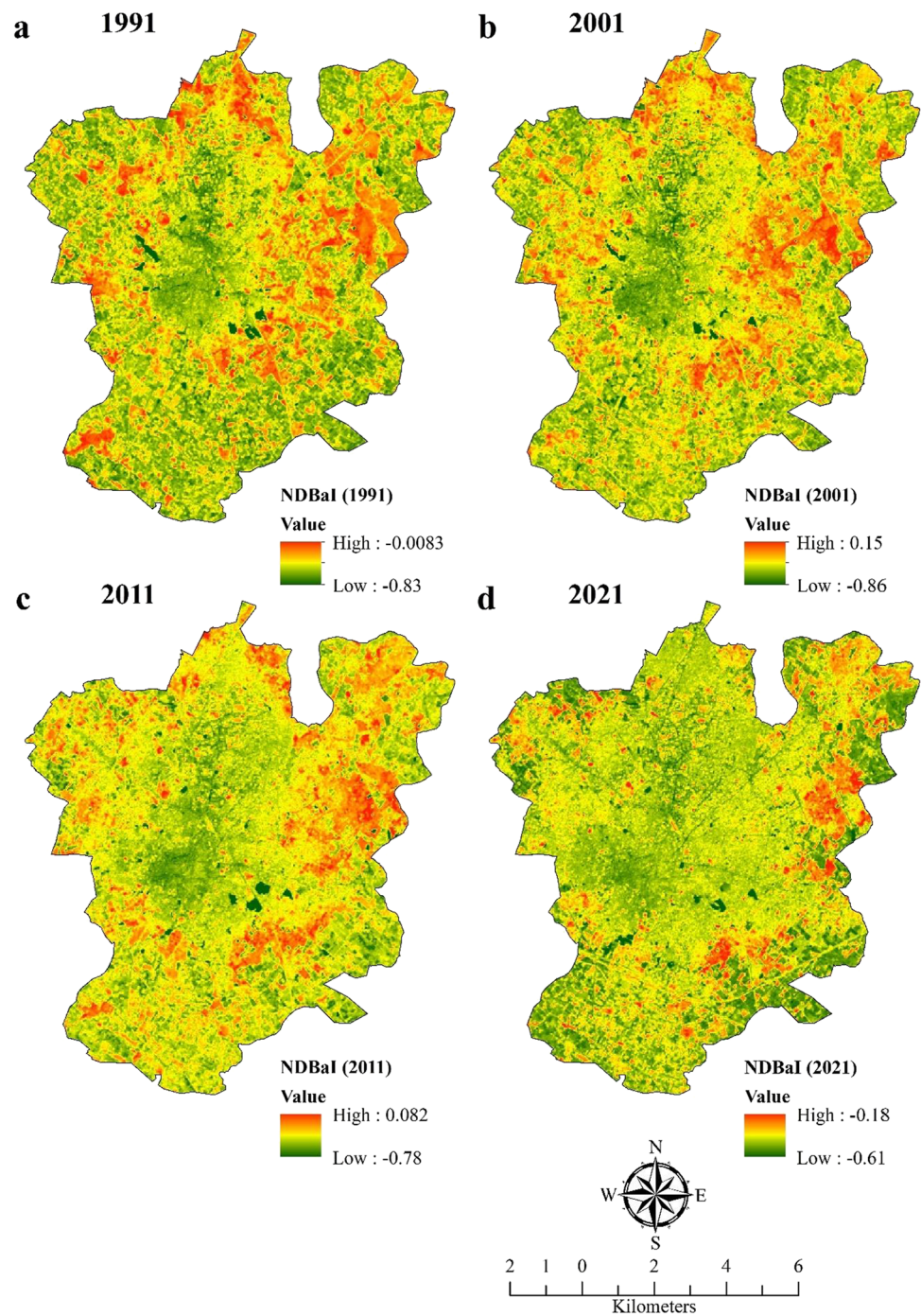
**Regression analysis**

In this study, relationship has shown among different variables. To show the relationship, scatter plot with a linear regression line was used. MS Excel 2021 has been used to show the scatter plot by using the linear regression Eq. (13),

**Table 6** Area under different LST categories

LST	1991	2001	2011	2021
< 14	5.10	10.16	6.03	1.08
14–15	31.29	14.63	11.01	9.55
15–16	36.03	32.00	46.52	45.35
16–17	18.54	24.99	26.81	30.48
> 17	9.04	18.22	9.62	13.55

**Fig. 13** Normalized Difference Bareness Index (NDBaI) of Aligarh City (1991, 2001, 2011, and 2021)



$$Y_c = a + b \quad (12)$$

where  $Y_c$  represents estimated value,  $a$  = y-intercept, and  $b$  = regression coefficient.

The constants  $a$  and  $b$  are determined by:

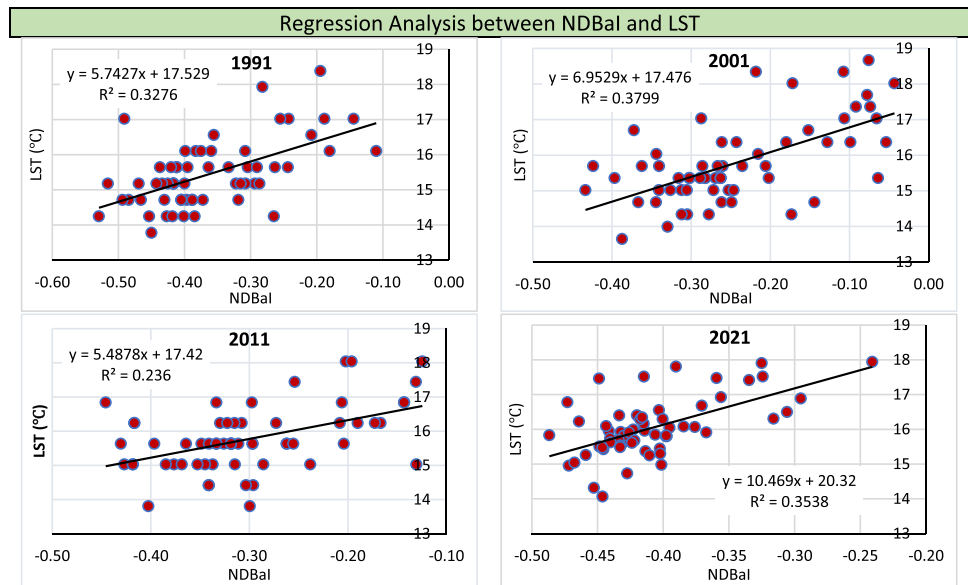
$$b = \frac{N \sum XY - \sum X \sum Y}{N \sum X^2 - (\sum X)^2}, a = \frac{\sum Y - b \sum X}{N} \quad (13)$$

### Accuracy assessment of LULC classification

The process of accuracy assessment and validation involves evaluating the accuracy of image classification by comparing it to ground truth locations and values. The following equation was used to validate the accuracy of classified raster maps:

$$\text{Overall accuracy (OA)} = \frac{\text{Number of true positive} + \text{number of true negative}}{\text{Pixels in the ground truth}} \times 100 \quad (14)$$

**Fig. 14** Plot of NDBaI vs LST with coefficient of determination ( $R^2$ ) for different time periods



The Kappa coefficient ( $k$ ) is a technique used to evaluate the level of agreement between multiple observers in the classification of discrete variables. It is a multivariate technique that has been used for accuracy assessment purposes, as described by Cohen (1960). The Kappa coefficient is a useful measure for assessing the inter-observer agreement among classified classes, as described by Foody (1992).

$$\text{Cohen's Kappa coefficient } (\hat{k}) = \frac{n \sum_{i=1}^r x_{ii} - \sum_{i=1}^r (x_i - x_{+i})}{n^2 - \sum_{i=1}^r (x_i - x_{+i})} \quad (15)$$

In a matrix with “ $r$ ” being the number of rows, “ $x_{ii}$ ” represents the number of observations in the “ $i$ th” row and column. The marginal totals of row “ $i$ ” and column “ $i$ ” are denoted as “ $x_i$ ” and “ $x_{+i}$ ”, respectively. “ $n$ ” represents the total number of observations (samples/pixels).

To validate the accuracy of four satellite images taken in 1991, 2001, 2011, and 2021, which were classified into five classes of land use/land cover (built-up, vegetation, water body, agriculture, and fallow land), 200 training sample points were obtained from Google Earth and topographical sheets for these years.

Supervised image classification has been used for the process of land use/land cover maps. Firstly, the satellite data (i.e., Landsat 5 TM, Landsat 7 ETM+, Landsat-5 TM, and Landsat 8 OLI) have been downloaded from <https://earthexplorer.usgs.gov/> and imported into the ArcGIS 10.5 software then created composite band and extracted area of interest (AOI).

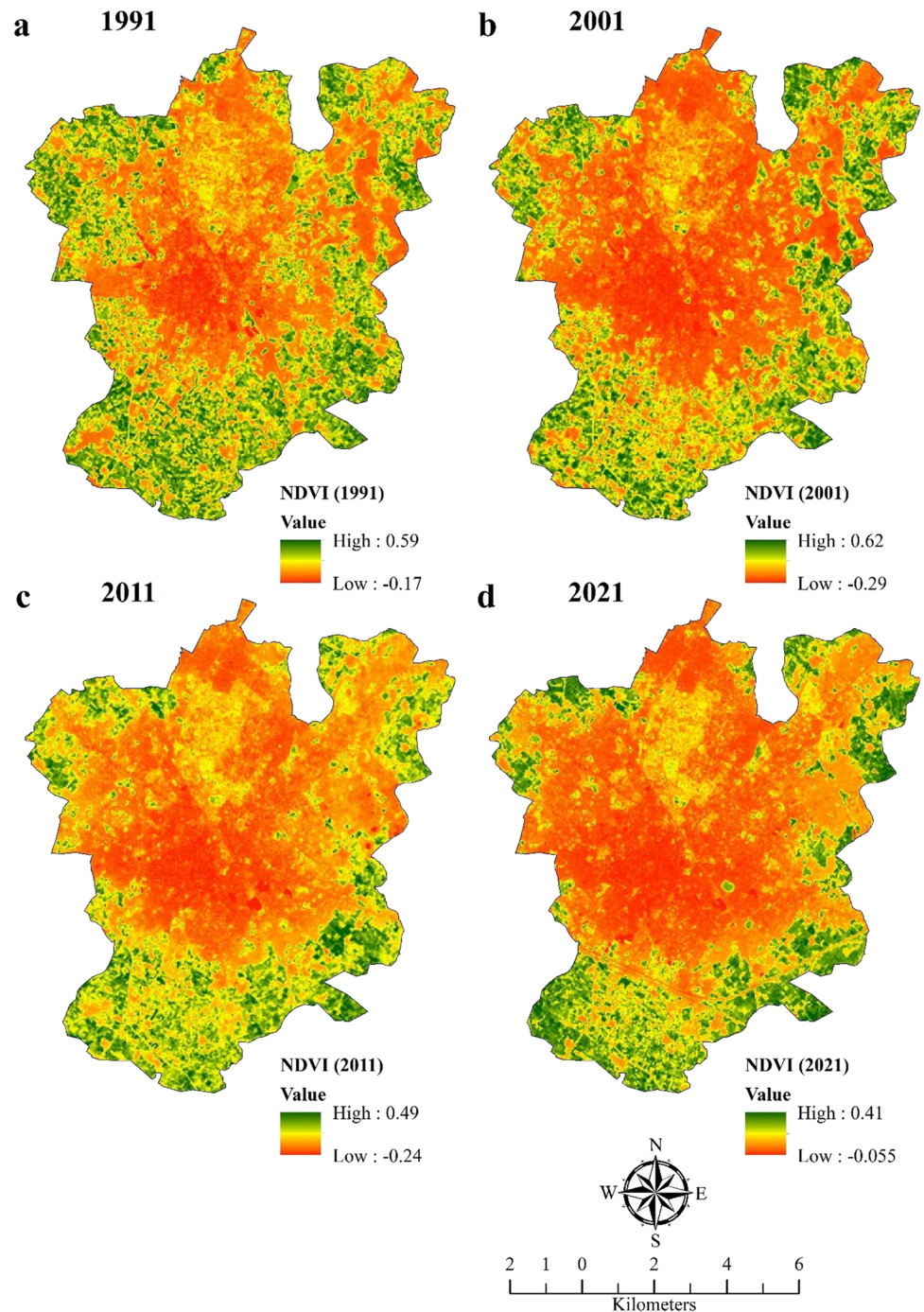
## Results and discussion

### Land transformation analysis

The study focused on the dominant land transformation of Aligarh city, generating six major classes. Other classes with small proportions were not clearly reflected and were therefore incorporated into neighboring classes within the system. The resulting classification products offer an overview of the primary land use characteristics in Aligarh city and its surrounding areas in 1991, 2001, 2011, and 2021. The data provided includes comprehensive information on different land use areas, as well as spatial and temporal transformations, transformation rates, and trends in increasing or decreasing land use patterns. The total area covered was 9861.21 ha, and accuracy assessments of the classification images were conducted using 179 reference pixels for each time period. The overall accuracy was found to be 80%, 85%, 87%, and 88% for 1991, 2001, 2011, and 2021, respectively, with Kappa coefficients of 0.7433, 0.8157, 0.8400, and 0.8270 (Fig. 4 and Table 2).

Over time, the precision of land transformation images has increased because more detailed and higher resolution reference maps have become available. Other researchers, including Sexton et al. (2013) and Rawat et al. (2013), have also conducted comparable image classification and post-classification.

**Fig. 15** Normalized Differentiate Vegetation Index (NDVI) of Aligarh City (1991 and 2021)



### Change detection of land use land cover types

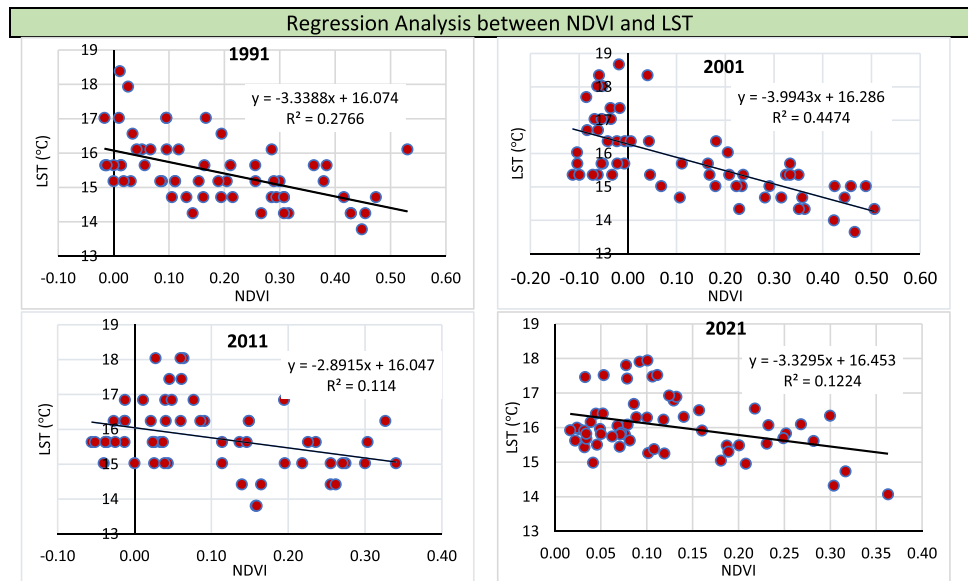
According to the definition provided by Hoffer (1978), change detection analysis refers to the examination of temporal effects resulting from variations in spectral response. This occurs when the spectral properties of vegetation or other types of cover in a particular area change over time. To address this issue, technology needs to be advanced, and the possibilities in various areas of

application are virtually limitless. This can be addressed using earth monitoring satellite data and decision support tools such as the Geographic Information System (GIS) (ESCAP 2016) (Table 3).

Changes in land use and land cover (LULC) for 1991, 2001, 2011, and 2021, were analyzed (Table 5, Figs. 5 and 6), and it was found that urban areas had rapidly expanded, with the built-up area increasing from 15.62 to 23.65% during 1991–2001 and then 41.55% to 53.03% in 2011–2021.



**Fig. 16** Plot of NDVI vs LST with coefficient of determination ( $R^2$ ) for different time periods



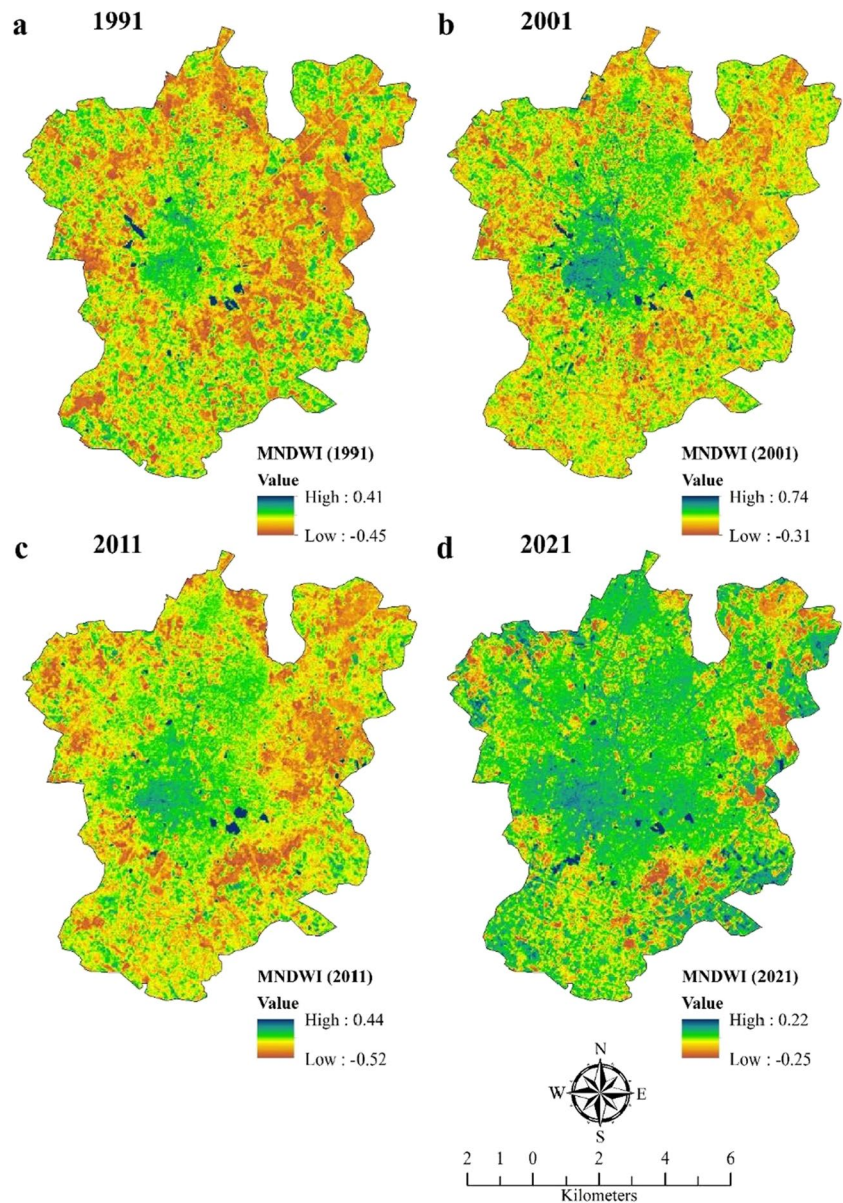
Meanwhile, fallow/bare land decreased from 34.21 to 31.95% in the first decade and then further decreased to 20.50 to 18.43% in the second decade. The area of cropland also decreased significantly, with the proportion falling from 40.76% in 1991 to 33.78% in 2001. Furthermore, it continued to decrease and became 27.21% in 2011 and 19.88% in 2021. Also, from the Fig. 6, it is clear that the only human-induced land use that has demonstrated a positive shift or a steady rise in built-up and vegetation, with a coefficient of determination ( $R^2$ ) value of 0.982 and 0.9511. This is in stark contrast to other categories such as cropland, bare land, vegetation, and water bodies. These categories have all exhibited a negative shift, having the respective ( $R^2$ ) values of 0.9996, 0.9093, 0.8962, and 0.9987. This suggests that these land use types have been decreasing over time, while only built-up and plantation shows an increasing trend. This suggests that factors such as urbanization, infrastructural growth, and government initiatives to promote plantation may be contributing to the positive growth of these two classes. Urbanization is a significant driver in the built-up areas. As cities like Aligarh experience growth and economic development, there is a need for more residential and industrial spaces. This leads to the expansion of built-up areas to accommodate the growing demands of the urban. Even infrastructural growth, such as construction of roads, bridges, and buildings, can also contribute to the increase in built-up areas. As the city develops and expands its infrastructure, more land is converted to built-up areas to support these developments. Additionally, government initiatives to promote plantation could be the reason for its positive growth. Governments often implement programs to encourage afforestation, reforestation, and sustainable agricultural practices.

These initiatives could be subsidies, training programs, and awareness campaigns to encourage individuals and organizations to engage in plantation. Such can lead to an increase in the area dedicated to plantations.

The vegetated area and water bodies also decreased, while the area under plantation increased to 4.42% (Fig. 4, Table 3). Specifically, between 1991 and 2021, there was a 239.56% increase in urban built-up area and a decrease of 51.23%, 46.13%, 54.23%, and 23.28% in cropland, bare land, vegetation, and water bodies, respectively. It can also be noticed that the majority of cropland and bare land (11.63% and 21.13%, respectively) have been converted into urban built-up area as shown in Fig. 4 and Table 3. Overall, the results indicate that the expansion of urban areas happened at the expense of cropland and bare land in all directions, with a majority of these lands being converted to urban built-up areas. The primary area where significant changes occurred was the urban zone, where there was a consistent conversion of other types of land into impermeable built-up areas. Land used for agriculture and wetlands located near the urban area were highly vulnerable to being altered by the construction of buildings and plantation. In urban areas that were closer to the city center, agricultural land was overtaken by urban development, while more distant land was transformed into plantation. All the results clearly show that a lot of transformations have taken place in the study area. Also, in the last three decades, there has been a transition of population from village to city areas.

The paper also includes tables on LULC transformation matrix (Table 3) and map (Fig. 7) and accuracy assessments of land cover types as shown in Table 4 (Figs. 8, 9, 10, and 11).

**Fig. 17** Modified Normalized Differentiate Water Index (NDWI) of Aligarh City (1991 and 2021)



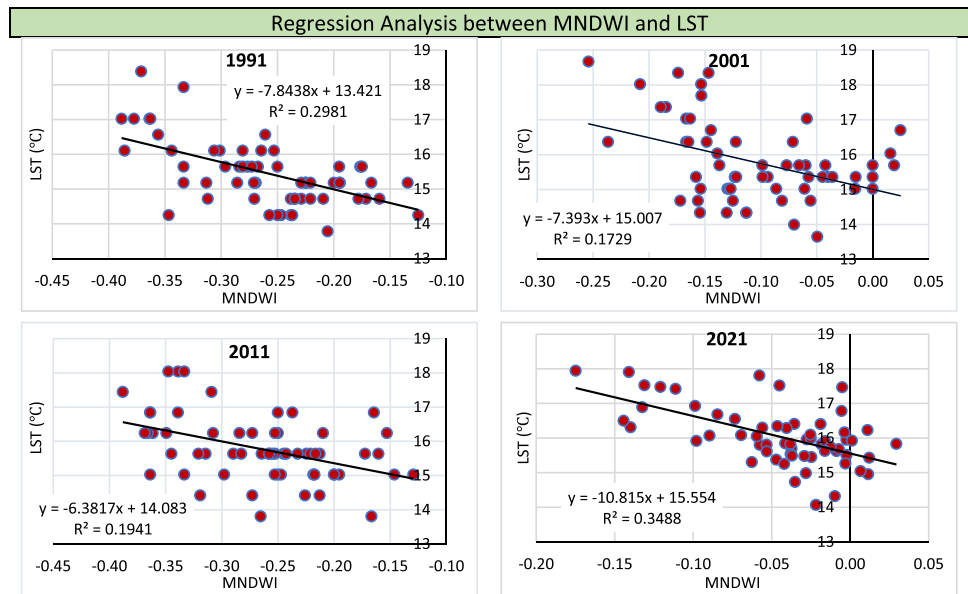
### Land surface temperature change

Figure 12 highlights an analysis of the spatial and temporal patterns of land surface temperature (LST) in four phases, namely, 1991, 2001, 2011, and 2021. The maps highlight areas of higher and lower temperatures, indicating the concentration and shift of LST patterns, which are linked to changes in land use and land cover. The analysis shows that the core urban area is sensitive to high temperatures, and there has been an arithmetic increase in mean LST of around  $0.62\text{ }^{\circ}\text{C}$  since 1991–2021, with a mean decadal increase rate of  $0.31\text{ }^{\circ}\text{C}$  from 1991 to 2001,  $0.04\text{ }^{\circ}\text{C}$  from 2001 to 2011, and  $0.27\text{ }^{\circ}\text{C}$  from 2011 to 2021 (Table 5).

This paper also presents a spatial analysis of land surface temperature (LST) over four phases—1991, 2001, 2011, and

2021—using maps with reddish tones highlighting higher temperature and green tones indicating lower LST. The analysis is conducted in the month of January in decadal years to identify changes in LST concentration and temporal shifts in LST patterns indicating rapid land use/land cover change (LULCC). The study shows that LST concentration ranges from  $12.84$  to  $20.18\text{ }^{\circ}\text{C}$  (Table 5) in January 1991, with 36% of the study area having temperatures ranging from  $15$  to  $16\text{ }^{\circ}\text{C}$  while 9.04% of the area having temperatures more than  $17\text{ }^{\circ}\text{C}$  (Table 6, Fig. 9). Similarly, for January 2001, the temperature ranges between  $12.60$  to  $20.27\text{ }^{\circ}\text{C}$  with 32% of the area having a temperature of  $15$  to  $16\text{ }^{\circ}\text{C}$  and 18.22% of the area lying in a temperature zone of more than  $17\text{ }^{\circ}\text{C}$  (Table 6, Fig. 9). For the year 2011, the minimum and maximum temperature ranges between  $12.57$  and  $20.41\text{ }^{\circ}\text{C}$ , with

**Fig. 18** Plot of MNDWI vs LST with coefficient of determination ( $R^2$ ) for different time periods



46.52% of the area lying in a temperature zone of 15–16 °C and 9.62% of the area lies in a maximum temperature zone (Table 6, Fig. 9). Finally, for 2021, it is estimated that the temperature ranges between 13.40 and 21.40 °C. The maximum area of 45.35% lies in the 15–16 °C temperature zone, while 13.55% of the area lies in the maximum temperature zone of 17 °C (Table 6, Fig. 9). The core urban area is found to be sensitive to high temperatures. The maximum and minimum LST patterns have increased in these subsequent phases, with the minimum LST increasing from 12.84 to 13.40 °C and the maximum temperature increasing from 20.18 to 21.40 °C since 1991 (Table 5).

The study area’s eastern and western regions close to the periphery show a relatively high temperature range due to the concentration of bare land and built-up area. The study period of 40 years shows a rise of 0.56 °C in the minimum temperature level, with an average increase of 0.54 °C/year (Table 5). A few patches in the southeastern and southwestern parts of the study area have relatively low temperature ranges, possibly due to the presence of water bodies and plantations. The result shows that the major proportion of an area concentration has shifted towards higher temperature classes in the later phases. This means that a greater proportion of the area has been experiencing enhanced temperatures.

From Fig. 10, it can be assessed that in AA’, the temperature is moderate all over the area, showing a slightly higher temperature in the extreme southern periphery due to the presence of barren land. Additionally, the temperature is low near the waterbody. From BB’, it is evident that the temperature is higher in the barren land compared to other areas, while a comparatively low temperature could be seen in the central part due to the presence of

the university area. From CC’, it can be assessed that an extremely high temperature prevails in the area away from the core of the city where the concentration of barren land is maximum. Furthermore, an extreme rise in the maximum temperature could be seen radiating from the center of the city in the four decades from 1991 to 2021 due to the expansion of the urban area.

### Temperature changes in built-up area

Several scientists have discovered a strong correlation between high temperatures and areas with dense populations, heavy industrialization, and many buildings. To investigate the urban heat island effect, they utilized Landsat TM/ETM+ images, as well as NDVI and NDBI indices. Their research found that impermeable surfaces are associated with elevated land surface temperatures (LST). Furthermore, some researchers argue that a lack of vegetation coverage also contributes to the urban heat island effect (Xiao et al. 2007; Weng et al. 2004). Figure 11 depicts the intensity and spatial distribution of built-up and impervious land in 1991, 2001, 2011, and 2021, as represented by NDBI classes. The expansion and intensity of this land have increased over time due to population growth and urbanization. Figure 12 demonstrates the correlation between NDBI and LST from 1991 to 2021, with a linear regression model fitted in all four instances. The coefficients of determination values for these four decades are 0.4108, 0.5214, 0.2382, and 0.3522, all of which strongly suggest that NDBI scores have a positive impact on LST. The rising trend of the  $R^2$  value in 1991–2001 and 2011–2021 confirms that high-intensity impervious land has the maximum LST. Conversely, negative control was observed in one decade ( $R^2=0.5214$  in 2001 and 0.2382 in 2011) between NDBI and LST (Fig. 12).

The Normalized Difference Bareness Index (NDBaI) is used to assess the level of bare soil or barrenness in a given area. It ranges from  $-1$  to  $1$ , where values close to  $1$  indicate areas with a high amount of bare land, values close to  $0$  indicate areas with a balanced distribution of vegetation and bare land, and values close to  $-1$  indicate areas with a high amount of vegetation. Figure 13 shows the NDBaI classes, which reveal the extent of impervious surfaces such as paved areas and buildings that are typically associated with lower values of vegetation and higher values of bare land. It can also be used to monitor changes in land cover and land use over time and to assess the impact of urbanization on the environment. The maximum values of NDBaI for the four decades, i.e., 1991, 2001, 2011, and 2021, are  $-0.0083$ ,  $0.15$ ,  $0.082$ , and  $-0.18$ , respectively (Fig. 13). Therefore, it clearly supports the idea that areas with high temperatures are largely linked to changes happening in urban areas, as well as in vegetation, barren land, and open spaces. As a result, the urbanization and thermal conditions of a city are primarily linked to the amount of developed urban space and bare land, while the presence of vegetation cover tends to reduce these effects.

Figure 14 shows the regression analysis between NDBaI and LST for the years 1991–2021. Based on the coefficient of determination values, it is revealed that for the year 1991, the  $R^2$  value is  $0.3276$ , which increased to  $0.3799$  in 2001, further decreased to  $0.236$  in 2011, and finally reached  $0.3538$  in 2021. All the values strongly indicate that there is a positive correlation between NDBaI and LST.

### Temperature changes in vegetated land

It is an evident fact that vegetation cover is extremely essential, as a single large tree can transpire  $450$  L of water per day, which consumes  $1000$  MJ of heat energy to drive the evaporation process. In this way, trees in the city can lower the summer temperatures of the particular area (Bolund and Hunhammar 1999). The above NDVI maps (Fig. 15) show that the AMU green campus, located centrally upward, has a high NDVI value compared to its surroundings and experiences low LST. They also display the spatial arrangement of NDVI categories, which were derived from multi-temporal satellite imagery. This classification was carried out to establish a connection between the NDVI values of various intensity levels and LST. The alteration of cropping patterns, the reduction of agricultural land, the relocation of water hyacinths, continuous expansion of built-up areas, and the increase of plantation are the key factors that have contributed to changes in NDVI over time. The findings of this study align with previous research, which suggests that a higher LST is associated with a lower NDVI (Fig. 15). In 1991, the NDVI values ranged between  $0.59$  and  $0.17$ , and in 2001, they ranged from  $0.62$  to  $0.29$ . Furthermore, in 2011,

they ranged between  $0.49$  and  $0.24$ , and ultimately, in 2021, they ranged between  $0.41$  and  $0.055$  (Fig. 15). Therefore, it can be inferred that NDVI has decreased in the urban core over time. As documented in previous studies, the relationship between NDVI and LST is negative, and the  $R^2$  value for January 1991 is  $0.2766$ , which changes to  $0.4474$  in 2001. Then, in 2011, it further changes to  $0.114$  and finally becomes  $0.12249$  (Fig. 16). Figure 16 displays the pattern of NDVI classes extracted from multi-temporal satellite images. This classification was performed to establish a relationship between NDVI and LST, which is affected by various factors, including changes in cropping patterns, agricultural land use, water hyacinth relocation, built-up expansion, and an increase in plantation. The research findings indicate that higher LST values are associated with lower NDVI levels (Fig. 16). So overall, it can be documented that there is a negative relationship between LST and NDVI over time and space.

### Temperature changes in water bodies

Water bodies generally have lower temperatures than other land uses and possess cooling properties. In the city, they help to even out temperature deviations during summer and winter. To explore this relationship, 60 samples were taken using a systematic sampling technique and correlated with LST. It was found that MNDWI is highly correlated with LST. The relationship between the proportion of water bodies, mean water body size, the proportion of the largest water patch in the landscape, the isolation, and fragmentation of water bodies and mean LST is negative. This means that regions with lower ratios of water bodies, smaller water bodies, and more isolated and fragmented water bodies tend to have higher mean LST values. The maximum MNDWI varies over time, with values of  $0.41$  in 1991,  $0.74$  in 2001,  $0.44$  in 2011, and  $0.21$  in 2021 (Fig. 17). Figure 18 shows that MNDWI has a negative impact on LST for different periods. In January, between 1991 and 2001, the  $R^2$  value decreased ( $R^2=0.2981$  in 1991,  $0.1729$  in 2001), which may be attributed to the penetration of radiation to the greatest depth of the water bodies due to their shallowing as the temperature increased. Conversely, from 2001 to 2011 and 2011 to 2021, the  $R^2$  values ( $0.1729$  in 2001,  $0.1941$  in 2011, and  $0.3488$  in 2021) indicate a growing controlling power of water bodies on LST.

### Association with different intra LULC classes

#### Intra LULC indices

The preceding discussion highlights that each types of land use and land cover (LULC) has its own distinct pattern of surface temperature, and its response varies by year. In the

following section, we will investigate how different intensities of a single type of LULC can affect surface temperature. For instance, built-up land tends to have the highest temperature, but the radiant surface within built-up areas can vary depending on the intensity of development in different parts of an urban area. This phenomenon also applies to the depth and quality of water bodies and the intensity and extent of vegetated areas, as well as to bare land. With this in mind, we will conduct a temperature analysis specific to each type of LULC. We have derived four land cover indices, namely NDBI, NDBaI, NDVI, and MNDWI to establish quantitative relationships between LST and these indices. According to the above regression analysis (Figs. 12, 14, 16, and 18), it can be said that NDVI, MNDWI, and LST are negatively related, while NDBI and NDBaI are positively related to LST. Built-up areas have a significant impact on land surface temperature and contribute to the formation of the urban heat island. In contrast, urban ecological services like urban forests, parks, road trees, and water bodies minimize the effect of urban heat islands or decrease land surface temperature. This implies that urban growth has an impact on LST since non-evaporating, non-transpiring surfaces like stone, metal, and concrete were used in place of natural vegetation (Zekarias et al. 2017).

## Conclusion

The findings of this study indicate that Aligarh City has undergone significant urban expansion, resulting in an increase in land surface temperature (LST) and the formation of an urban heat island. The similar results could be found in an urban center of English Bazar, Malda, and in the city of Lucknow conducted by Pal and Ziaul (2017), Singh et al. (2017), and Shukla and Jain (2021). There was a similar problem of urbanization and climate change prevalent in these urban centers because of the continuous expansion in the urban dwellings as well as land transformations taking place abruptly. The changing land use patterns, including the conversion of agricultural land and vegetation into built-up areas, and the transformation of water bodies have contributed to the rise in temperature in the urban fringe areas. Our analysis shows that the blue-green infrastructure has a negative impact on UHIs, which will likely intensify with rapid urbanization, making it challenging to reverse. However, growth management policies such as the implementation of green belts, new urbanism concepts such as green buildings and horticulture-based plants on rooftops, and a revision of vacant space policies between buildings, implementing sustainable farming, recycling, and composting organic waste, capturing methane from landfills, carbon capture and storage. Reducing greenhouse gas emissions and promoting

sustainability can help in minimizing the effect of UHIs. Keeping a check on land use changes, such as deforestation and urbanization, which can contribute to rising land surface temperatures, and implementing sustainable irrigation practices can further help in reducing LST. It is also important to conserve water bodies and wetlands to some extent to slow down the temperature increase. Encouraging urban population dispersion towards peripheral areas and preserving free earthen spaces with less concrete structures can also help mitigate the impact of rising temperatures. For the city to have a healthy urban environment, we firmly advocate for the balancing of vegetative groups (such as grasses, shrubs, and trees) with diffused built infrastructure (such as buildings, highways, and parking areas). Given that urbanization cannot be stopped, but can be sensibly rerouted with meticulous planning, management, and policy execution, this study is an attempt to guide the planners for sustainably designing the policies considering the temperature changes. Therefore, continuous monitoring of land use and cover changes and the development of rational, scientific, and sustainable urban land use policies are necessary to prevent the intensification of the UHI phenomenon. By implementing these measures, we can create a more sustainable and liveable environment for the people of Aligarh City.

Our research shows that the primary driver of urban heat island development in the region is unplanned growth. Urban planners and policymakers can use this technique to identify significantly the city's highly impacted locations and the causes that affect them. The work serves as an example of the importance of urban elements in monitoring LST's influence, which is crucial to urban planning. But the present research has certain limitations as it does not take into account the impact of seasonal and nocturnal variations in the surface temperatures. Secondly, it examined the connection between LST, factors influencing it, environmental indicators, and expansion over a specific time frame. When considering the spatial variety of the landscape, a scale impact arises that causes variance. As a result, it is crucial that future researches should take into account multi-seasonal and diurnal data in order to examine the variations in surface temperature.

**Funding** Financial support from the Indian Council of Social Science Research (ICSSR), Government of India, (F. No. 02/6909/OBC/2021–22/ICSSR/RP/MJ) is greatly acknowledged.

**Data Availability** Data availability will be with the corresponding author on reasonable request.

## Declarations

**Competing interests** The authors declare no competing interests.

## References

- Abbas A, He Q, Jin L, Li J, Salam A, Lu B, Yasheng Y (2021) Spatio-temporal changes of land surface temperature and the influencing factors in the Tarim basin, Northwest China. *Remote Sens* 13(19). <https://doi.org/10.3390/rs13193792>
- Ahmad WS, Jamal S, Taqi M, El-Hamid HTA, Norboo J (2022) Estimation of soil erosion and sediment yield concentrations in Duhganga watershed of Kashmir Valley using RUSLE and SDR model. *Environ Dev Sustain* 1–24
- Al-sharif AA, Pradhan B (2014) Monitoring and predicting land use change in Tripoli Metropolitan City using an integrated Markov chain and cellular automata models in GIS. *Arab J Geosci* 7:4291–4301
- Arnfield AJ (2003) Two decades of urban climate research: a review of turbulence, exchanges of energy and water, and the urban heat island. *Int J Climatol* 23(1):1–26. <https://doi.org/10.1002/joc.859>
- Arora MK, Das Gupta AS, Gupta RP (2004) An artificial neural network approach for landslide hazard zonation in the Bhagirathi (Ganga) Valley, Himalayas. *Int J Remote Sens* 25(3):559–572
- Arsanjani JJ, Helbich M, Kainz W, Boloorani AD (2013) Integration of logistic regression, Markov chain and cellular automata models to simulate urban expansion. *Int J Appl Earth Obs Geoinf* 21:265–275
- Behera DK, Jamal S, Ahmad WS, Taqi M, Kumar R (2023) Estimation of soil erosion using RUSLE model and GIS tools: a study of Chilika Lake, Odisha. *J Geol Soc India* 99(3):406–414
- Bolund P, Hunhammar S (1999) Ecosystem services in urban areas. *Ecol Econ* 29(2):293–301. [https://doi.org/10.1016/S0921-8009\(99\)00013-0](https://doi.org/10.1016/S0921-8009(99)00013-0)
- Cohen J (1960) A coefficient of agreement for nominal scales. *Educ Psychol Meas* 20(1):37–46. <https://doi.org/10.1177/001316446002000104>
- ESCAP U (2016) Making an impact: innovative HRD approaches to poverty alleviation. *Fire Rescue Magazine*, 34(6). <https://hdl.handle.net/20.500.12870/3831>
- Foody GM, Campbell NA, Trodd NM, Wood TF (1992) Derivation and applications of probabilistic measures of class membership from the maximum-likelihood classification. *Photogramm Eng Remote Sensing* 58(9):1335–1341
- Ganaie TA, Jamal S, Ahmad WS (2021) Changing land use/land cover patterns and growing human population in Wular catchment of Kashmir Valley, India. *GeoJournal* 86:1589–1606
- Hoffer RM (1978) Biological and physical considerations in applying computer-aided analysis techniques to remote sensing. *Remote Sensing: The Quantitative Approach*, pp 227–289. <https://cir.nii.ac.jp/crid/1570854175786961920.bib?lang=en>
- Hulley GC, Ghent D, Göttsche FM, Guillevic PC, Mildrexler DJ, Coll C (2019) Land surface temperature. In *Taking the temperature of the Earth* (57–127). Elsevier
- Imhoff ML, Zhang P, Wolfe RE, Bounoua L (2010) Remote sensing of the urban heat island effect across biomes in the continental USA. *Remote Sens Environ* 114(3):504–513. <https://doi.org/10.1016/j.rse.2009.10.008>
- Jamal S, Ahmad WS (2020) Assessing land use land cover dynamics of wetland ecosystems using Landsat satellite data. *SN Appl Sci* 2:1–24
- Jamal S, Ahmad WS, Ajmal U, Aaquib M, Ashif Ali M, Babor Ali M, Ahmed S (2022a) An integrated approach for determining the anthropogenic stress responsible for degradation of a Ramsar site–Wular Lake in Kashmir, India. *Marine Geodesy* 45(4):407–434
- Jamal S, Malik IH, Ahmad WS (2022b) Dynamics of urban land use and its impact on land surface temperature (LST) in Aligarh City, Uttar Pradesh. In *Re-envisioning advances in remote sensing* (25–40). CRC Press
- Jamali AA, Kalkhajeh RG, Randhir TO, He S (2022) Modeling relationship between land surface temperature anomaly and environmental factors using GEE and Giovanni. *J Environ Manage* 302:113970
- Khursheed V, Jamal S, Ahmad WS (2022) Impact assessment of land use land cover dynamics and population growth on food security of Kashmir Valley, India. *Towards sustainable natural resources: monitoring and managing ecosystem biodiversity*. Springer International Publishing, Cham, pp 123–149
- Li X, Yeh AGO (2002) Neural-network-based cellular automata for simulating multiple land use changes using GIS. *Int J Geogr Inf Sci* 16(4):323–343
- Liu H, Weng Q (2012) Enhancing temporal resolution of satellite imagery for public health studies: a case study of West Nile virus outbreak in Los Angeles in 2007. *Remote Sens Environ* 117:57–71. <https://doi.org/10.1016/j.rse.2011.06.023>
- Liu L, Zhang Y (2011) Urban heat island analysis using the Landsat TM data and ASTER data: a case study in Hong Kong. *Remote Sens* 3(7):1535–1552. <https://doi.org/10.3390/rs3071535>
- Mallick J, Kant Y, Bharath BD (2008) Estimation of land surface temperature over Delhi using Landsat-7 ETM+. *J Ind Geophys Union* 12(3):131–140
- Meyer WB, Turner BL (1992) Human population growth and global land-use/cover change. *Annu Rev Ecol Syst* 23(1):39–61
- Mishra VN, Rai PK (2016) A remote sensing aided multi-layer perceptron-Markov chain analysis for land use and land cover change prediction in Patna district ( Bihar ), India. *Arab J Geosci*. <https://doi.org/10.1007/s12517-015-2138-3>
- Naikoo MW, Rihan M, Ishtiaque M (2020) Analyses of land use land cover (LULC) change and built-up expansion in the suburb of a metropolitan city: spatio-temporal analysis of Delhi NCR using Landsat datasets. *J Urban Manag* 9(3):347–359
- Oke TR, Cleugh HA (1987) Urban heat storage derived as energy balance residuals. *Bound-Layer Meteorol* 39(3):233–245. <https://doi.org/10.1007/BF00116120>
- Pal S, Akoma O (2009) Water scarcity in wetland area within Kandi block of West Bengal: a hydro-ecological assessment. *Ethiopian J Environ Stud Manag* 2(3). <https://doi.org/10.4314/ejesm.v2i3.48260>
- Pal S, Ziaul SK (2017) Detection of land use and land cover change and land surface temperature in English Bazar urban centre. *Egypt J Remote Sens Space Sci* 20(1):125–145
- Puyravaud JP (2003) Standardizing the calculation of the annual rate of deforestation. *For Ecol Manage* 177(1–3):593–596. [https://doi.org/10.1016/S0378-1127\(02\)00335-3](https://doi.org/10.1016/S0378-1127(02)00335-3)
- Qin Z, Karnieli A, Berliner P (2001) A mono-window algorithm for retrieving land surface temperature from Landsat TM data and its application to the Israel-Egypt border region. *Int J Remote Sens* 22(18):3719–3746. <https://doi.org/10.1080/01431160010006971>
- Rahaman N, Baratin A, Arpit D, Draxler F, Lin M, Hamprecht FA, Bengio Y, Courville A (2019) On the spectral bias of neural networks. *36th Int Conf Mach Learn ICML 2019* 2019-June(1):9230–9239
- Rawat JS, Biswas V, Kumar M (2013) Changes in land use/cover using geospatial techniques: A case study of Ramnagar town area, district Nainital, Uttarakhand, India. *Egypt J Remote Sens Space Sci* 16(1):111–117
- Roberts DA, Batista GT, Pereira JLG, Waller E, Nelson BW (1998) Change identification using multitemporal spectral mixture analysis: Applications in eastern Amazonia. *Environmental Monitoring Applications, Remote Sensing Change Detection*, pp 137–161

- Sahana M, Rihan M, Deb S, Patel PP, Ahmad WS, Imdad K (2020) Detecting the facets of anthropogenic interventions on the palaeochannels of Saraswati and Jamuna. In *Anthropogeomorphology of Bhagirathi-Hooghly river system in India* (469–489). CRC Press
- Sang L, Zhang C, Yang J, Zhu D, Yun W (2011) Simulation of land use spatial pattern of towns and villages based on CA–Markov model. *Math Comput Model* 54(3–4):938–943
- Sexton JO, Song XP, Feng M, Noojipady P, Anand A, Huang C, Townshend JR (2013) Global, 30-m resolution continuous fields of tree cover: Landsat-based rescaling of MODIS vegetation continuous fields with lidar-based estimates of error. *Int J Digital Earth* 6(5):427–448
- Shahfahad, Mourya M, Kumari B, Tayyab M, Paarcha A, Asif, Rahman A (2021) Indices based assessment of built-up density and urban expansion of fast growing Surat city using multi-temporal Landsat data sets. *GeoJournal* 86:1607–1623
- Sharma A, Vashishtha D (2023) Spatio-temporal assessment of land use land cover changes and their impact on variations of land surface temperature in Aligarh Municipality. *J Indian Soc Remote Sens* 2. <https://doi.org/10.1007/s12524-022-01652-2>
- Shen X, Liu B, Jiang M, Lu X (2020) Marshland loss warms local land surface temperature in China. *Geophys Res Lett* 47(6):e2020GL087648
- Shukla A, Jain K (2021) Analyzing the impact of changing landscape pattern and dynamics on land surface temperature in Lucknow city, India. *Urban For Urban Green* 58:126877
- Singh P, Kikon N, Verma P (2017) Impact of land use change and urbanization on urban heat island in Lucknow city, Central India. A remote sensing based estimate. *Sustain Cities Soc* 32:100–114. <https://doi.org/10.1016/j.scs.2017.02.018>
- Smith GM, Spencer T, Murray AL, French JR (1998) Assessing seasonal vegetation change in coastal wetlands with airborne remote sensing: an outline methodology. *Mangrove Salt Marshes* 2:15–28
- Talukdar S, Singha P, Mahato S, Pal S, Liou YA, Rahman A (2020) Land-use land-cover classification by machine learning classifiers for satellite observations—a review. *Remote Sens* 12(7):1135
- Thomas E, Michail F, Julie G, Güneralp B, Marcotullio PJ, McDonald RI, Parnell S, Schewenius M, Sendstad M, Seto KC, Wilkinson C (2013) Regional assessment of Africa. In *Urbanization, biodiversity and ecosystem services: challenges and opportunities: a global assessment*. [https://doi.org/10.1007/978-94-007-7088-1\\_23](https://doi.org/10.1007/978-94-007-7088-1_23)
- Tran DX, Pla F, Latorre-Carmona P, Myint SW, Caetano M, Kieu HV (2017) Characterizing the relationship between land use land cover change and land surface temperature. *ISPRS J Photogramm Remote Sens* 124:119–132
- United Nation (DESA) Department of Economic and Social Affairs, 2018. Revision of World Urbanization Prospects. <https://www.un.org/development/desa/publications/2018-revision-of-world-urbanization-prospects.html>
- UN-Habitat (2020) World cities report 2020. <https://doi.org/10.18356/c41ab67e-en>
- Vinayak B, Lee HS, Gedam S, Latha R (2022) Impacts of future urbanization on urban microclimate and thermal comfort over the Mumbai metropolitan region, India. *Sustain Cities Soc* 79(2021):103703. <https://doi.org/10.1016/j.scs.2022.103703>
- Weng Q, Lu D, Schubring J (2004) Estimation of land surface temperature-vegetation abundance relationship for urban heat island studies. *Remote Sens Environ* 89(4):467–483. <https://doi.org/10.1016/j.rse.2003.11.005>
- Xiao RB, Ouyang ZY, Zheng H, Li WF, Schienke EW, Wang XK (2007) Spatial pattern of impervious surfaces and their impacts on land surface temperature in Beijing. *J Environ Sci (China)* 19(2):250–256
- Zekarias A, Taddele H, Zenebe A (2017) Influence of climate variables on vector and prevalence of bovine trypanosomosis in Tselemti District, North West Tigray, Ethiopia. In *Climate change management*. [https://doi.org/10.1007/978-3-319-49520-0\\_19](https://doi.org/10.1007/978-3-319-49520-0_19)
- Zhao L, Lee X, Smith RB, Oleson K (2014) Strong contributions of local background climate to urban heat islands. *Nature* 511(7508):216–219. <https://doi.org/10.1038/nature13462>

Springer Nature or its licensor (e.g. a society or other partner) holds exclusive rights to this article under a publishing agreement with the author(s) or other rightsholder(s); author self-archiving of the accepted manuscript version of this article is solely governed by the terms of such publishing agreement and applicable law.